AD-A089 414 MATERIALS SCIENCES CORP BLUE BELL PA F/G 11/6
ELEVATED TEMPERATURE BEHAVIOR OF METAL- MATRIX COMPOSITES.(U)
MAY 80 Z HASHIN, E A HUMPHREYS F49620-79-C-0059
UNCLASSIFIED MSC/TPR/1130/1502 AFOSR-TR-80-0936 NL

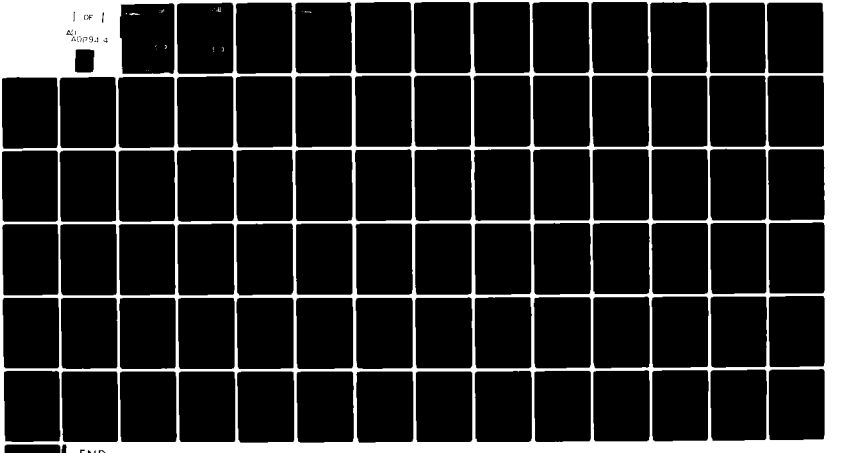

END
DATE FILMED
10-80
DTIC

Materials Sciences Corporation

(5)

LEVEL II

ELEVATED TEMPERATURE BEHAVIOR OF METAL-MATRIX COMPOSITES

MSC TPR 1130/1502

May, 1980

Unclassified

SECURITY CLASSIFICATION OF THIS PAGE (When Data Entered)

5 LEVEL II

REPORT DOCUMENTATION PAGE

READ INSTRUCTIONS BEFORE COMPLETING FORM

1. REPORT NUMBER: AFOSR-TR-80-0936	2. GOVT ACCESSION NO.: AD-A089414
3. RECIPIENT'S CATALOG NUMBER	
4. TITLE (and Subtitle): Elevated Temperature Behavior of Metal-Matrix Composites.	5. TYPE OF REPORT & PERIOD COVERED: Interim progress rpt. 1 Apr 79 — 31 Mar 80 Interim
	6. PERFORMING ORG. REPORT NUMBER: MSC/TPR/1130/1502
7. AUTHOR(s): Zvi Hashin, E. A. Humphreys	8. CONTRACT OR GRANT NUMBER(s): F49620-79-C-0059
9. PERFORMING ORGANIZATION NAME AND ADDRESS: Materials Sciences Corporation, Blue Bell Office Campus, Merion Towle House, Blue Bell, PA 19422	10. PROGRAM ELEMENT, PROJECT, TASK AREA & WORK UNIT NUMBERS: 2307/B1, 61102F
11. CONTROLLING OFFICE NAME AND ADDRESS: Air Force Office of Scientific Research, Building 410, Bolling AFB, DC 20332	12. REPORT DATE: May 1980
	13. NUMBER OF PAGES: 77
14. MONITORING AGENCY NAME & ADDRESS (if different from Controlling Office)	15. SECURITY CLASS. (of this report): Unclassified
	15a. DECLASSIFICATION/DOWNGRADING SCHEDULE

16. DISTRIBUTION STATEMENT (of this Report)

Approved for public release, distribution unlimited

17. DISTRIBUTION STATEMENT (of the abstract entered in Block 20, if different from Report)

DISTRIBUTION STATEMENT A
Approved for public release;
Distribution Unlimited

DTIC ELECTE SEP 22 1980 S D B

18. SUPPLEMENTARY NOTES

19. KEY WORDS (Continue on reverse side if necessary and identify by block number)

Metal Matrix Composites
Graphite Fibers
Plasticity
Temperature Dependent
Numerical Analysis
Stress-Strain Curves

20. ABSTRACT (Continue on reverse side if necessary and identify by block number)

An elasto-plastic, temperature-dependent analysis of a graphite/aluminum composite material system was performed. A hexagonal array model was utilized along with a numerical analysis procedure. Results for the transversly isotropic material included residual processing effects and stresses, and temperature dependent, one-dimensional stress-strain relations, utilizing both isotropic hardening and kinimatic hardening assumptions for aluminum matrix.

DD FORM 1 JAN 73 1473 EDITION OF 1 NOV 65 IS OBSOLETE 390991

Unclassified

20. The data generated have shown considerable influence of the residual processing stresses upon both the room temperature and elevated temperature stress-strain response to the material.

Materials Sciences Corporation

ELEVATED TEMPERATURE BEHAVIOR OF METAL-MATRIX COMPOSITES

Technical Progress Report

MSC TPR 1130/1502

May, 1980

Prepared by:

Zvi Hashin
E. A. Humphreys

Prepared for:

Air Force Office of Scientific Research
Bolling Air Force Base, D.C. 20332

Contract F49620-79-C-0059

Blue Bell Office Campus, Merion Towle House, Blue Bell, Pennsylvania 19422 • 215 542-8400

TECHNICAL PROGRESS REPORT
April 1, 1979 - March 31, 1980

The present report summarizes the research effort by the Materials Sciences Corporation on the analysis of temperature-dependent stress-strain relations of metal-matrix composites (MMC) during the period April 1, 1979 through March 31, 1980. The work done is part of a comprehensive program to provide analytical tools for the evaluation of thermomechanical properties and internal stresses of unidirectional MMC and their laminates. This program consists of the following parts:

1. Analytical determination of one-dimensional temperature dependent stress-strain relations on the basis of micromechanics.
2. Determination of temperature-dependent stress-strain relations for combined states of stress in terms of one-dimensional stress-strain relations on the basis of macro-incremental theory.
3. Establishment of laminate analysis methods incorporating the stress-strain relations for combined states of stress.

This report is concerned with part (1) of the program.

Approved by:

B. Walter Rosen
Program Manager

TABLE OF CONTENTS

INTRODUCTION. 1

MODELING AND APPROACH. 3

GENERALIZED PLANE STRAIN. 5

ANTI-PLANE STRAIN. 5

NUMERICAL ANALYSIS. 6

APPROXIMATE TREATMENT. 9

RESULTS. 12

ELASTIC ANALYSIS. 12

INELASTIC THERMOMECHANICAL ANALYSIS. 13

Isotropic Hardening. 13

Kinematic Hardening. 18

CONCLUSION. 22

REFERENCES. 24

APPENDIX A - ANSYS PLASTICITY. 26

TABLES. 31

FIGURES. 36

INTRODUCTION

The usual metal-matrix composite consists of an aluminum alloy matrix and carbon or graphite (sometimes boron) fibers. The metal matrix is a temperature dependent elasto-plastic material. The fibers are anisotropic and elastic throughout the whole temperature range and may be described as transversely isotropic with respect to their longitudinal axes. In view of the large longitudinal stiffness of the fibers, it may be assumed that no significant average plastic strain can develop in fiber direction and the Poisson induced transverse strain associated with uniaxial stress in fiber direction is also elastic. It follows that the loadings which are most significant in terms of macro-plasticity and non-linearity are: stress transverse to fibers; transverse shear; and axial shear. Consequently, the chief concern will be to evaluate temperature dependent macro stress-strain relations for these cases.

The problem of the prediction of the macro stress-strain relations of such a composite is one of very great difficulty. General treatments such as those for elastic and viscoelastic composites are not available. Treatments given in the literature are generally concerned with the isothermal case. Unless otherwise stated, all work to be cited below is of such nature.

A general qualitative discussion of elasto-plastic composites has been given in reference 1. Limit analysis treatments which are only concerned with prediction of ultimate loads for ideally plastic matrix have been given in references 2 and 3. A numerical treatment to compute the stress-strain relation for transverse uniaxial stress for a limited strain range has been given in reference 4, based on the idealized geometry of a square array fiber model. A similar approach but including interaction between shear and transverse load has been given in reference 5. A micromechanics stress analysis for a square array has been given in reference 6. The self consistent scheme approximation has been utilized in reference 7 for the case of rigid fibers and elasto-plastic matrix characterized by isotropic J_2 deformation theory. This was

generalized in reference 8 to include fiber elasticity; all this for transverse loading only. Significant work to predict initial yield surfaces has been given in references 9, 10, and 11, including temperature change but primarily for axisymmetric states.

All of the treatments available describe important special cases but they are not sufficient to define the needed one-dimensional temperature dependent stress-strain relations of a unidirectional MMC.

MODELING AND APPROACH

The unidirectional composite may be considered transversely isotropic in the macro sense since the fibers are randomly placed. For the purpose of micromechanics analysis, it is necessary to represent the MMC by some suitable model. Two models which comply with transverse isotropy are the composite cylinder assemblage (CCA) (refs. 12,13) figure 1, and the periodic hexagonal array, figure 2. Both of these models have been used to compute elastic properties of fiber composites, the first in terms of analytical results and the second by numerical analysis. Available results show that the predictions of these models are numerically very close and agree quite well with experimental data. It is therefore believed that either one of them can be used in the present, much more complicated situation. However, in the present elastoplastic case, the CCA model can be utilized analytically only for axisymmetric states of applied stress; i.e., uniaxial stress combined with transversely isotropic stress. This loading does not exhibit significant plastic strains. For other loadings, analytical solution of the CCA model is not feasible. It is therefore necessary to turn to numerical analysis and in this respect the hexagonal array of equal fibers is a more attractive model than the CCA. Therefore, the present analysis will be based on the hexagonal array model.

In this respect it should be noted that the frequently employed square array model is not suitable since it is not transversely isotropic.

For the purpose of evaluation of the stress-strain relations, we consider a prismatic specimen of square cross section (fig. 3) in which the fibers are in the generator direction and arranged in a hexagonal array (fig. 2). Loadings to be considered are uniaxial transverse stress $\bar{\sigma}_{22}$ (or $\bar{\sigma}_{33}$), transverse shear $\bar{\sigma}_{23}$, and axial shear $\bar{\sigma}_{12}$, as illustrated in figure 4; all of these at various temperatures.

The one-dimensional effective stress-strain relations may be written as:

$$d\bar{\varepsilon}_{22} = \frac{d\bar{\sigma}_{22}}{E^*_{Tt}} \tag{1}$$

$$d\bar{\varepsilon}_{22} = \frac{d\bar{\sigma}_{23}}{2G^*_{Tt}} \tag{2}$$

$$d\bar{\varepsilon}_{12} = \frac{d\bar{\sigma}_{12}}{2G^*_{At}} \tag{3}$$

where E^*_{Tt}, G^*_{Tt}, and G^*_{At} are temperature-dependent effective tangent moduli and overbars denote averages.

If the specimen is heated without load, the free effective tangent thermal expansion coefficient α^*_{Tt} is defined by:

$$d\bar{\varepsilon}_{22} = d\bar{\varepsilon}_{33} = \alpha^*_{Tt} d\phi \tag{4}$$

where $d\phi$ is temperature increment.

In order to compute the constitutive relations (eqns. 1-4) it is necessary to compute average strain increments produced by average stress increments (eqns. 1-3) and temperature increments (eqn. 4). For this purpose it is necessary to determine the micro-strain fields in the fibers and matrix of the hexagonal array model, thus to solve a succession of elasto-plastic boundary value problems for successive load and temperature increments. In these boundary value problems the fibers are transversely isotropic elastic and the matrix is elasto-plastic. Displacement and traction continuity must be satisfied at fiber/matrix interfaces at all times. Once the displacement field is known, the strain field is obtained by differentiation and the average strain increments can be determined.

For the purpose of the analysis performed here, it is sufficient to consider the cases of generalized plane strain and anti-plane strain. These are defined as follows:

GENERALIZED PLANE STRAIN

Traction Boundary Conditions

$$T_1(S) = \sigma^{o}_{11} n_1$$

$$T_2(S) = \sigma^{o}_{22} n_2 + \sigma^{c}_{23} n_3 \qquad (5)$$

$$T_3(S) = \sigma^{o}_{23} n_2 + \sigma^{o}_{33} n_3$$

where n_i are the components of the normal to the surface and 1 is fiber direction. These boundary conditions include uniaxial stress in fiber direction, uniaxial stress in direction transverse to fibers, and transverse shear.

The internal displacements have the forms:

$$\left.\begin{aligned} u_1 &= \varepsilon_o x_1 \\ u_2 &= u_2(x_2, x_3) \\ u_3 &= u_3(x_2, x_3) \end{aligned}\right\} \quad \text{in fibers and matrix} \qquad (6)$$

ANTI-PLANE STRAIN

Traction Boundary Conditions

$$T_1(S) = \sigma^{o}_{12} n_2 + \sigma^{o}_{13} n_3$$

$$T_2(S) = \sigma^{o}_{12} n_1 \qquad (7)$$

$$T_3(S) = \sigma^{o}_{13} n_1$$

These boundary conditions are suitable for axial shear.

The internal displacements have the forms:

$$\left.\begin{aligned} u_1 &= u_1(x_2,x_3) \\ u_2 &= \varepsilon^o_{12}x_1 \\ u_3 &= \varepsilon^o_{13}x_1 \end{aligned}\right\} \quad \text{in fibers and matrix} \qquad (8)$$

NUMERICAL ANALYSIS

Analytical treatment of the problem is not feasible and therefore numerical analysis is performed. It is recalled that the matrix is elasto-plastic and temperature dependent. Only a small number of computer programs which are suitable for such a situation are available. Of these the most attractive appears to be the ANSYS (ref. 14) finite element program which was selected for the present analysis.

In view of the periodicity of the problem, it is sufficient to carry out the analysis for a typical repeating element. Such an element is shown in figure 5. The boundary conditions on its faces can be determined by symmetry considerations and the type of external loading applied. Such boundary conditions suitable for finite element analysis are shown in figure 6 for transverse extension (compression) and in figure 8 for axial shear. In addition, displacement and traction boundary conditions at fiber/matrix interfaces must be satisfied at all times.

It should be noted that all of the boundary value problems are two-dimensional, thus requiring only two-dimensional finite elements. The ANSYS program, however, requires that the model be created utilizing three-dimensional elements. The model is the constrained in such a fashion that a two-dimensional problem is formed. Division of the repeating element into finite elements is shown in figure 9.

The fibers (carbon or graphite) are transversely isotropic elastic. Their thermo-elastic stress-strain relations are:

$$\varepsilon_{11} = \frac{\sigma_{11}}{E_A} - \frac{\nu_A}{E_A}\sigma_{22} - \frac{\nu_A}{E_A}\sigma_{33} + \alpha_A\phi$$

$$\varepsilon_{22} = -\frac{\nu_A}{E_A}\sigma_{11} + \frac{\sigma_{22}}{E_T} - \frac{\nu_T}{E_T}\sigma_{33} + \alpha_T\phi$$

$$\varepsilon_{33} = -\frac{\nu_A}{E_A}\sigma_{11} - \frac{\nu_T}{E_T}\sigma_{22} + \frac{\sigma_{33}}{E_T} + \alpha_T\phi \qquad (9)$$

$$\varepsilon_{12} = \frac{\sigma_{12}}{2G_A}$$

$$\varepsilon_{23} = \frac{\sigma_{23}}{2G_T}$$

$$\varepsilon_{13} = \frac{\sigma_{13}}{2G_A}$$

where

E_A - axial Young's modulus;

E_T - transverse Young's modulus;

ν_A - axial Poisson's ratio;

ν_T - transverse Poisson's ratio;

G_A - axial shear modulus;

G_T - transverse shear modulus

α_A - axial thermal expansion coefficient;

α_T - transverse thermal expansion coefficient.

In the generalized plane strain formulation (eqn. 5), $\sigma_{12} = \sigma_{13} = 0$; while in the anti-plane strain formulation (eqn. 7), $\sigma_{11} = \sigma_{22} = \sigma_{33} = \sigma_{23} = 0$.

The matrix (aluminum) is elasto-plastic and its general incremental stress-strain relations are not precisely known. Two important extreme cases are isotropic hardening and kinematic hardening. In both cases the initial yield surface is described by the Mises condition:

$$S_{ij}S_{ij} = \sigma_y^2/3 \tag{10}$$

where S_{ij} is the stress deviator and σ_y is the (temperature dependent) yield stress in simple uniaxial stress. Isotropic hardening assumes that the yield surface expands in stress space retaining its initial shape; kinematic hardening assumes that the yield surface translates in stress space retaining its initial shape and dimensions. The ANSYS computer program has the capability to handle both of these cases.

The incremental solution procedure is as follows: At a given loading specified by tractions T_i^o and temperature ϕ, the internal stresses and strains are σ_{ij} and ε_{ij}. Now loads and temperature are changed by amounts ΔT_i^o and $\Delta\phi$. The corresponding stress and strain increments $\Delta\sigma_{ij}$ and $\Delta\varepsilon_{ij}$ are determined by a sequence of iterations so as to satisfy equilibrium, compatibility, plasticity stress-strain relations, traction and displacement continuity at fiber/matrix interfaces and external loading boundary conditions. The increments $\Delta\sigma_{ij}$ and $\Delta\varepsilon_{ij}$ are dependent on the current states of stress and strain. Once these increments have been determined, their addition to the current stresses and strains produces a new current state and the next increments are computed. The initial states of stress and strain are the elastic fields at first occurrence of plastic strains. A summary of the ANSYS plasticity procedure for isotropic and kinematic hardening is given in the appendix. The procedure is also illustrated by the flow chart of figure 10.

The plasticity input into the ANSYS procedure is the one-dimensional elasto-plastic stress-strain relation. For the purpose of the numerical analysis, it is necessary to approximate the

curved stress-strain relations by linear segments. This is shown in figure 11 for temperature dependent simple tensile stress-strain relations of aluminum 2024, approximated by three linear segments.

APPROXIMATE TREATMENT

As has been mentioned before, a successful analysis of elastic properties of fiber composites has been given on the basis of the composite cylinder assemblage (CCA) model (refs. 12,13). The analysis has been generalized to the case of transversely isotropic constituents (ref. 15) which is of importance for carbon and graphite fibers.

For the case of transversely isotropic fibers and isotropic matrix, some of the relevant CCA results are:

Transverse Shear Modulus

$$G_T^* = G_m \left[1 + \frac{v_f(1+\beta_m)}{\zeta - v_f\left[1+\frac{3v_m^2\beta_m^2}{\alpha v_f^3 - \beta_m}\right]}\right] \tag{11}$$

where

$$\alpha = \frac{\beta_m - \gamma\beta_f}{1 + \gamma\beta_f}$$

$$\zeta = \frac{\gamma + \beta_m}{\gamma - 1}$$

$$\gamma = \frac{G_{TF}}{G_m}$$

$$\beta_m = \frac{1}{3 - 4\nu_m} \qquad \beta_f = \frac{k_F}{k_f + 2G_{Tf}}$$

where M_m, M_f indicate matrix and fiber elastic moduli. The assumption is made that when the matrix deforms plastically, the tangent effective modulus is given approximately by:

$$M_t^* = F[M_{mt}(\bar{\sigma}_m),\ M_f,\ v_f] \tag{16}$$

where $\bar{\sigma}_m$ is the matrix average of the stress component corresponding to the applied stress component (e.g., pure transverse shear when dealing with effective transverse tangent shear modulus) and $M_{mt}(\bar{\sigma}_m)$ is the matrix tangent modulus at value $\bar{\sigma}_m$.

It may then be shown that the matrix average stress increment $d\bar{\sigma}_m$ and the applied average stress increment $d\bar{\sigma}$ are related by:

$$d\bar{\sigma}_m = \frac{d\bar{\sigma}}{v_m} \frac{M_f/M_t^* - 1}{M_f/M_{mt}(\bar{\sigma}_m) - 1} \tag{17}$$

where M_t^* is the function (eqn. 16). The relation (eqn. 17) defines the stress increment $d\bar{\sigma}_m$ in terms of current average stress $\bar{\sigma}_m$.

In order to evaluate the tangent modulus (eqn. 16) $\bar{\sigma}_m$ is first computed for the beginning of plastification. Then as the applied external load is increased, successive $d\bar{\sigma}_m$ are determined by equation 17. Thus the value of $\bar{\sigma}_m$ for every applied $\bar{\sigma}$ is known and M_t^* is then defined by equation 16.

The approximate treatment outlined has been applied to the prediction of the effective axial shear stress-strain relation. Since the aluminum stress-strain relations have been approximated by linear segments (see fig. 11) equation 17 also gives a linear segment approximation. The comparison is shown in figure 12 and it is seen that the approximation is excellent.

Transverse Young's Modulus

$$E_T^* \approx \frac{4k^*G_T^*}{k^* + G_T^*} \tag{12}$$

where k^* is the effective transverse bulk modulus given by:

$$k^* = \frac{k_m(k_f+G_m)v_m + k_f(k_m+G_m)v_f}{(k_f+G_m)v_m + (k_m+G_m)v_f} \tag{13}$$

Axial Shear Modulus

$$G_A^* = G_m \frac{G_m v_m + G_{Af}(1+v_f)}{G_m(1+v_f) + G_{Af}v_m} . \tag{14}$$

In these expressions,

m - indicates matrix
f - indicates fiber
v - volume fraction
G_m - matrix shear modulus
k_m - matrix plane strain bulk modulus
G_{Tf} - fiber transverse shear modulus
G_{Af} - fiber axial shear modulus
k_f - fiber transverse bulk modulus.

Let any of the effective elastic moduli (refs. 11-14) be denoted:

$$M_c^* = F(M_m, M_f, v_f) \tag{15}$$

RESULTS

ELASTIC ANALYSIS

The numerical procedures for generating one-dimensional elasto-plastic temperature dependent stress-strain curves for metal-matrix composites are quite time consuming. As a result, it is impractical to utilize these non-linear results to check the accuracy and validity of the finite element model. It was deemed appropriate, therefore, to perform a series of elastic analyses to verify the finite element model.

It is very important to choose a proper finite element mesh size. If the size is too large the results will not be accurate; if the size is too small too much computer time will be expended. The finite element scheme shown in figure 9 consisting of 212 elements, has been utilized to obtain effective elastic moduli of the unidirectional composite. The same computations were then performed with a finer mesh consisting of 322 elements. Effective moduli obtained with the two meshes gave a maximum difference of 0.4%. This verifies the accuracy of the mesh chosen.

The elastic properties which were used in the generalized plane strain and anti-plane analyses are listed in table 1. The properties correspond to a 2024-T4 aluminum matrix material and T-50 graphite fibers. The aluminum alloy was chosen simply because the most complete set of properties were available for it. The T-50 fiber was used as this is the fiber most commonly used in graphite/aluminum material systems.

The elastic moduli predicted for the composite based upon the properties in table 1 are listed in table 2. Two different computational schemes were used in the calculations. These were the finite element analysis and models described previously, and the composite cylinder assemblage (CCA), see references (12, 13). It is well known that hexagonal array results and CCA results are numerically very close.

This is also verified by the present results as seen from table 2. This may be considered as a demonstration of the accuracy of the finite element model and analysis.

INELASTIC THERMOMECHANICAL ANALYSIS

The finite element model developed and verified in the previous sections was utilized to predict one-dimensional, temperature dependent, elasto-plastic, stress-strain curves for the metal-matrix material system under consideration. The predictions were made with the elastic constants defined previously for the graphite fibers and with temperature dependent stress-strain curves input for the aluminum matrix. Analyses were performed under both isotropic and kinematic hardening assumptions for the matrix material.

Isotropic Hardening

The initial series of analyses of metal-matrix composites were performed under the isotropic hardening assumption with regard to the matrix material. The input data consisted of linearly segmented stress-strain curves for the aluminum. Curves of this type were input for each of five different temperatures ranging from 21°C to 377°C. The set of curves input representing the aluminum matrix are shown in figure 11. The thermal expansion data used for the aluminum are plotted and shown in figure 13.

The program used for these analyses was ANSYS, which is a multi-purpose finite element code. The assumptions and conditions utilized in the computerized analyses are very significant for evaluation of the predicted curves and for comparisons of the curves generated under the two hardening assumptions. For this reason, a brief description of the ANSYS plasticity calculations is included in an appendix.

Thermal Expansion

The first analyses performed under the isotropic hardening assumption were free thermal expansions. Figures 14 and 15 depict the transverse and axial response of the graphite/aluminum system, respectively. Included in these figures are the

cooldown from the stress-free temperature to room temperature and a re-heat to the stress-free temperature. In addition, elastic, temperature dependent free thermal expansion curves are presented in the figures. The plastic analyses involved six temperature increments in both the cooling and heating paths.

Examination of the data in the curves indicates that no significant yielding occurs during cooling until the temperature drops to nearly 150°C. The re-heat curves in both figures are totally elastic, thus explaining their similarity in shape to the elastic predictions. At the room temperature state, considerable plastic yielding was predicted by the analysis. The matrix stresses in the axial direction averaged over 350 MPa, while the fiber axial stresses averaged over -830 MPa. These are very high stresses, indicating considerable plastic deformation and expansion of the yield surface.

In each of the predicted stress-strain responses presented in this report, the prior load history began at the stress free temperature, unless otherwise stated. Thus, curves presented as room temperature response include the effects of cooling the material from the stress free temperature. Curves which represent elevated temperature response include not only the initial cooldown but also the effects of re-heating to the stated temperature. Only those curves noted as having no processing stresses correspond to loadings from a microscopically stress free state.

Transverse Normal Loading

The material response to transverse normal loadings is shown in figures 16, 17 and 18. Figure 16 presents the normal stress-strain response, while figures 17 and 18 show Poisson induced strains in the transverse plane and axial directions, respectively. Each of the three figures includes tensile and compressive loadings with the previous room temperature stress and strain field as the initial state. In addition,

a tensile loading curve with no thermal processing stresses is included for comparison.

The three figures demonstrate the significance of the residual thermal effects upon the stress-strain response. Comparison of the tensile and compressive curves at room temperature reveals considerable differences which are directly attributable to the processing stresses. The stress-strain curves of figure 16 indicte that the compressive response is more flexible than the tensile response. This is readily explained at the micromechanics level. Under tensile loading, significant portions of the model undergo unloading at low stress levels while the compressive loading produces further yielding at all load levels. When no initial yielding or stress is present, as in the tensile no processing stress run, the response was significantly stiffer.

The axial strain predictions demonstrate a curious response. The axial strain produced during transverse tensile loading from room temperature reverses direction. Again, the explanation lies within the micromechanics regime. As the material begins to yield significantly in tension, the large axial processing stresses begin to relieve themselves. Thus, the initial contraction due to the Poisson effect is followed by an expansion which tends to relieve the internal stresses. The compressive loading at room temperature produces the same axial effects but here the strains are additive and do not produce a reversal.

Temperature Effects on Transverse Loadings

In figures 19 and 20 the elevated temperature effects on the tensile stress-strain response is presented. The figures contain the room temperature response presented previously, as well as the tensile response at 204°C. The transverse stress-strain response in figure 19 indicates that significant yielding occurs at a higher stress at this elevated temperature. This is definitely contrary to what

would normally be expected. Considering the initial state of stress at room temperature resolves the quandary, however. The initial, large internal stresses at room temperature are relieved at the elevated temperature but the yield surface remains greatly expanded. In addition, the elastic modulus of the aluminum matrix material is only slightly (10%) reduced at 204°C. The combination of these effects produces a high temperature response with a slightly reduced initial slope but increased yield stress.

The Poisson induced strains in figure 20 show a similar effect. The two elevated temperature curves are nearly linear while the room temperature curves show the phenomenon described in a previous section.

The effects just described for the tensile response are also present in compression. Figures 21 and 22 present the compressive response at 204°C and the previously presented compressive curves at room temperature. Again, the elevated temperature stress-strain curve is slightly more flexible initially, but yields at a significantly higher load than the room temperature curve. The Poisson induced strains at elevated temperature are nearly linear while the room temperature curves are not.

Loading Effects on Thermal Expansion

The effects of mechanical loading on the thermal expansion response of the graphite/aluminum system is demonstrated in figures 23 and 24. In these figures, the free thermal expansion curves are those presented previously in figures 14 and 15. The curves generated with the applied mechanical stress have load histories consisting of the thermal cooling, followed by transverse tensile loading and finally, the re-heat shown in the figures.

The transverse expansion data are very interesting in that the material is not responding as a transversely isotropic body. The expansion in the direction of the mechanical load is much larger than in the direction perpendicular to the load. In addition, the mechanical loading has caused an increase

in the expansion in the loading direction and a decrease perpendicular to it with respect to the free thermal expansion case. The effects in the axial direction (figure 24) are simply a moderate decrease in the expansion due to temperature. In both figures, the applied mechanical load has reduced thermal expansions perpendicular to it due to Poisson induced strains associated with it. As the temperature increases and the elastic matrix modulus decreases, the strains are increased. Thus, the expansion in the loading direction increases and the perpendicular expansion decreases.

Load Path Effects

Since the effects of material plasticity are path dependent, comparisons of various load paths were made. The loadings involved included combinations of temperature and tensile transverse loads and combinations of temperature and compressive transverse loads. To facilitate these comparisons, two analyses were made where the loading was a simultaneous proportional variation of mechanical load and temperature. The tensile results of these runs are presented in figures 25 and 26 and the compressive results are shown in figure 27.

Comparisons of identical load states, arrived at along different paths, are presented in tables 3 and 4. The loadings of table 3 include transverse tension and temperature while the loadings in table 4 are transverse compression and temperture. In table 3, the data indicate that relatively low loadings produce less path dependence than higher loadings. This is of course to be expected, since the higher loadings produce more plastic effects. The data presented also indicate that in the range of loadings considered, superposition of mechanical and thermal loadings would produce reasonable accuracy. This would be of tremendous significance in simplifying the analysis of this material.

The data in table 4 demonstrate similar trends to the table 3 data. Here, as in the higher tensile loads data, the axial strain data show significant path dependence. The

magnitudes of the strains are very small, however, and the differences may be exaggerated by the numerical errors inherent in the solution process.

Shear

The shear response of the graphite/aluminum system under analysis is demonstrated in figures 28 through 30. The transverse shear response is depicted in figures 28 and 29 and the axial shear response is shown in figure 30.

The transverse shear stress-strain response is typical of the other room temperature transverse loadings. The interesting feature is the axial strain produced during the shear loading. This effect is due to the large, axial stresses developed during the initial cooldown. As the material yields in shear, the axial stresses relieve themselves causing the axial strain.

The axial shear response shown in figure 30 is not typical of the other curves presented. As was stated previously, the inclusion of the processing effects in the axial shear analysis would have required a three-dimensional analysis and was therefore not done. Since the axial shear loading originated on virgin material, the response is different. The most significant difference is the definite yield point present. All of the previous, room temperature solutions, yielded over a range of loading while the axial shear results indicate that most of the matrix material yields simultaneously.

Kinematic Hardening

The one-dimensional stress-strain responses of the graphite/aluminum system presented to this point have included the assumption of isotropic hardening with the aluminum matrix. Since the reversed loading behavior as modeled in ANSYS isotropic hardening is based upon an extension of one-dimensional plasticity (see Appendix) certain of the previous analyses were repeated utilizing a kinematic hardening assumption. These additional analyses also allow comparisons of the effects of the two hardening assumptions within the aluminum matrix, thus bracketing the reversed loading response of the composite.

Immediately, a difficulty arose in that the classical kinematic hardening utilized in ANSYS requires bi-linear stress-strain curves rather than the linearly segmented curves used for isotropic hardening. The only remedy was to model only the elastic and first plastic slopes of the isotropic input with the bi-linear kinematic input data. The stress-strain input curves for kinematic hardening are shown in figure 31. The thermal expansion data was identical to that used in the isotropic hardening. The mathematical constraints and conditions relating to the kinematic hardening used in ANSYS are discussed briefly in an included appendix.

Thermal Expansion

The first predictions of the composite response obtained with the kinematic hardening assumptions were the thermal expansion curves shown in figures 32 and 33. These figures also contain the curves predicted with the isotropic hardening assumption for comparison. The loading consisted of a cooldown from the stress-free temperature to room temperature, followed by a re-heat to the stress-free temperature. The data in the curves show two interesting phenomena. First, the cooldown curves are not identical, and secondly, at approximately 325°C in the re-heat analysis the kinematic hardening curves diverge significantly from the isotropic hardening curves. The first discrepancy is directly attributable to the differences in the isotropic and kinematic hardening input curves. The divergence at the higher temperatures during the process of re-heating can only be attributed to the difference in the hardening assumptions since the thermal loading is proportional.

In the isotropic hardening case, the yield surface was greatly expanded by the large internal stresses generated by the initial cooling process. For the kinematic process, the yield surface was greatly shifted during this cooling process but not expanded. The result of this difference is that while the isotropic hardening curves are well within

the yield surface at temperatures as high as the stress-free temperature, the kinematic hardening curves are not and therefore, yielding is occurring. This fundamental difference in the nature of the changing yield surface will manifest itself in most of the comparisons of isotropic hardening and kinematic hardening curves.

Transverse Normal Loading

The effects of the two hardening assumptions on the predicted transverse stress response curves are demonstrated in figures 34, 35 and 36. Due to the different input curves required, the results are only comparable to approximately 138 MPa. Beyond this stress, the average strains are above the second knee on the isotropic data and thus the results based on the two hardening assumptions begin to diverge.

Up to the point of divergence, both the stress-strain response of figure 34 and the transverse, Poisson induced strain curve of figure 35 are nearly identical for each type of hardening. The curves respond similarly as the internal stresses during the loading are predominantly increasing with respect to the thermal induced stresses already present. Therefore, the curves should be identical.

The Poisson induced axial strain response in figure 36 demonstrates the same effects as the other strain components, the difference being the stress level where the divergence occurs. The lower stress level here is undoubtedly due to the large axial residual stresses. These stresses magnify the differences in the hardening input curves as the material begins to yield.

Temperature Effects on Transverse Loading

Transverse tensile loading response, predicted at 204°C, is presented in figures 37, 38 and 39. These curves demonstrate a marked difference between the two hardening assumptions. The kinematic curves have a significantly reduced yield stress as compared with the isotropic curves.

This effect is strictly a function of the differing yield surfaces at the initial temperature state.

The isotropic hardening assumption causes the yield surface to expand in all directions in the stress space when yielding occurs while the kinematic assumptions shift the yield surface in the direction of the yielding stress component. Therefore, at room temperature, the kinematic hardening yield surface is shifted in the axial stress direction but not in the transverse stress direction, while the isotropic hardening yield surface is expanded in all stress directions. The results of this, coupled with the reduced axial residual stresses due to the elevated temperature, is the effect seen in these figures.

Load Path Effects

In order to evaluate the path effects upon the kinematic hardening results, simultaneous proportional tensile and thermal loadings were evaluated and the results are seen in figures 40, 41 and 42. These figures also have the comparable isotropic hardening data plotted on them. The lowered yield stress in the kinematic case has the explanation presented previously for the elevated temperature tensile data.

The comparison of the load path effects is listed in table 5. The differences here tend to be larger than for similar comparisons made for isotropic hardening (table 3). The difference of 15% in ε_2 is significant in that superposition of mechanical and thermal effects is probably not reasonable for this kinematic data.

The comparisons made here have shown significant dependence of the composite material response to the hardening assumptions for the matrix material.

The isotropic hardening results have been shown to be entirely consistent with the kinematic results.

CONCLUSION

It has been demonstrated that effective thermo-mechanical stress-strain relations of metal-matrix composites consisting of an elasto-plastic hardening matrix (aluminum alloy) and anisotropic (graphite or carbon) fibers can be obtained by finite element numerical analysis taking into account the significant temperature dependence of the matrix, three dimensional plasticity effects and residual stresses due to cooldown.

Use of isotropic hardening versus kinematic hardening plasticity has led to numerical differences in predicted stress-strain relations especially in the larger strain range. But it should be remembered that the nature of the computer program utilized, ANSYS, required different piece-wise linear approximations of plasticity stress-strain relations for isotropic and kinematic hardening. It is therefore felt that the question of the significance of numerical differences between effective stress-strain relations based on these different hardening assumptions merits further investigation.

An encouraging result of the analysis is seen in that the average strains produced by thermal expansion in the presence and in the absence of load are numerically close. This implied that for the materials and range of loadings considered the concept of the effective free thermal expansion coefficient remains valid for the composite having an elasto-plastic matrix, a result of extremely important practical significance.

A unique feature of the analyses performed here is their careful treatment of residual stresses. The specimens are actually only stress free at high temperature. When cooled down to room temperature they develop significant residual stresses and plastification of matrix. This has a significant effect upon stress-strain relations at room temperature.

In addition to the finite element analysis a simple approximate method for computation of effective stress-strain relations has been devised. Comparison of the results pre-

dicted by it with finite element analysis results for effective stress-strain relations in axial shear has shown excellent agreement. Consequently, the implications and utility of this approximation should be further investigated.

The work completed during this phase of the program has demonstrated the ability to compute one-dimensional stress-strain relations for metal-matrix composites under various combinations of thermal and mechanical loadings. The results obtained allow for significant insight and understanding of the one-dimensional response of the metal-matrix composite system under consideration.

Utilizing the composite material data predicted in the current effort, temperature dependent stress-strain relations for combined states of stress will be devised in the subsequent effort. These relations will be based upon a macro-incremental theory. Thus, the complete characterization of the mechanical and thermal response of a uni-directional metal-matrix lamina will be obtained. Following this, methods will be devised for incorporating these combined stress state relations into a laminate analysis methodology.

REFERENCES

1. Hill, R., "The Essential Structure of Constitutive Laws for Metal Composites and Polycrystals", J. Mech. Phys. Solids, 15, 79 (1967).

2. Hashin, Z., in NASA CR-207, (1965).

3. Shu, L.S. and Rosen, B.W., "Strength of Fiber Reinforced Composites by Limit Analysis Methods", J. Composite Materials, 1 , 366, (1967).

4. Adams, D.F., "Inelastic Analysis of a Unidirectional Composite Subjected to Transverse Normal Loading", J. Composite Materials, 4, 310 (1970).

5. Foye, R.L., "Theoretic Post Yielding Behavior of Composite Laminates, Part I - Inelastic Micromechanics", J. Composite Materials, 7, 178 (1973).

6. Lin, T.H., Salinas, D., and Ito, Y.M., "Elastic Plastic Analysis of Unidirectional Composites", J. Composite Materials, 6, 48 (1972).

7. Huang, W.C., "Plastic Behavior of Some Composite Matierals", J. Composite Materials, 5, 320 (1971).

8. Huang, W.C., "Elastoplastic Transverse Properties of a Unidirectional Fibre Reinforced Composite", J. Composite Materials, 7, 482 (1973).

9. Dvorak, G.J., Rao, M.S.M., and Tarn, J. Q., "Yielding in Unidirectional Composites under External Loads and Temperature Changes", J. Composite Materials, 7, 194 (1973).

10. Dvorak, G.J., Rao, M.S.M., and Tarn, J. Q., "Generalized Initial Yield Surfaces for Unidirectional Composites", J. Appl. Mech., 41, 249 (1974).

11. Dvorak, G.J., and Rao, M.S.M., "Axisymmetric Plasticity Theory of Fibrous Composites", Int. J. Engrg. Sci., 14, 361 (1976).

12. Hashin, Z. and Rosen, B.W., "The Elastic Moduli of Fiber Reinforced Materials", J. Appl. Mech., 31, 223, (1964).

13. Hashin, Z., "Theory of Fiber Reinforced Materials" NASA CR 1974, (1972).

14. Kohnke, P. "ANSYS Engineering Analysis System Theoretical Manual", Swanson Analysis Systems, Inc., (1977).

15. Hashin, Z., "Analysis of Properties of Fiber Composites With Anisotropic Constituents," J. of Appl. Mech., 46, 543 (1979).

APPENDIX A
ANSYS PLASTICITY

The finite element analysis code utilized in the current study was ANSYS. This is a proprietary computer code developed and maintained by Swanson Analysis Systems, Inc. ANSYS is a general multipurpose finite element code with many capabilities.

Two different hardening rules were used in the metal-matrix composite analysis. Both isotropic hardening and classical bilinear kinematic hardening were considered for the aluminum matrix material. The development of these two hardening rules is fundamentally different in ANSYS, even though the yield conditions (von Mises) and flow rules (Prandtl-Reuss) are identical. A brief synopsis of the pertinent elements of the derivations of the two plasticity approaches is given here. A more detailed description can be found in reference 14.

ISOTROPIC HARDENING

In ANSYS, isotropic hardening in two or more dimensions is developed as an extension of a one-dimensional case. The process involves computing equivalent, one-dimensional stresses and strains for evaluating the yield condition. The procedure is as follows.

First, a one-dimensional strain which includes plasticity effects is computed at iteration i.

$$\varepsilon_{e,i} = \frac{1}{\sqrt{2}\ (1+\nu_e)} \left\{ (\varepsilon_x^t - \varepsilon_y^t)^2 + (\varepsilon_y^t - \varepsilon_z^t) + (\varepsilon_z^t - \varepsilon_x^t) + \frac{3}{2}(\gamma_{xy}^t)^2 \right.$$

$$\left. + \frac{3}{2}(\gamma_{yz}^t)^2 + \frac{3}{2}(\gamma_{xz}^t)^2 \right\}^{1/2} \qquad \text{(A-1)}$$

where ε_j^t = total strain-thermal strain-origin shift strain.*

*An artificial strain which accounts for stress reversal, defined later.

This strain is compared to the previous maximum ε_{max} and loading is occurring if $\varepsilon_{e,i} > \varepsilon_{max}$. If this is the case, then ε_{max} is set equal to $\varepsilon_{e,i}$. Based on $\varepsilon_{e,i}$ and the input stress-strain curves, a one-dimensional equivalent stress, $\sigma_{e,i}$, is computed.

In equation A-1, ν_e is defined as:

$$\nu_{e,i} = \frac{1}{2} - \left(\frac{1}{2} - \nu\right) \frac{\sigma_{e,i}}{E\ \varepsilon_{e,i}} \tag{A-2}$$

thus, $\nu_{e,i}$ and $\varepsilon_{e,i}$ are related and the computation must be made iteratively. A quantity $(d\sigma_e/d\varepsilon_p)_{i-1}$ is now computed:

$$\left(\frac{d\sigma_e}{d\varepsilon_p}\right)_{i-1} = \frac{1}{\dfrac{\varepsilon_{e,i} - \varepsilon_{e,i-1}}{\sigma_{e,i} - \sigma_{e,i-1}} - \dfrac{1}{E}} \tag{A-3}$$

which is the rate of change of equivalent stress to plastic strain. Utilizing this, the plastic strain increment can be calculated.

$$\Delta\varepsilon_p = \frac{\varepsilon_{et} - \frac{2}{3}\frac{1+\nu}{E}\sigma_{e,i-1}}{\frac{2}{3}(1-\nu)\left(1+\frac{1}{E}\left[\frac{d\sigma_e}{d\varepsilon_p}\right]_{p,i-1}\right)} \tag{A-4}$$

where

$$\varepsilon_{et} = \frac{\sqrt{2}}{3}\left\{(\varepsilon_x' - \varepsilon_y')^2 + (\varepsilon_y' - \varepsilon_z')^2 + (\varepsilon_z' - \varepsilon_x')^2 + \frac{3}{2}(\gamma_{xy}')^2 + \frac{3}{2}(\gamma_{yz}')^2 + \frac{3}{2}(\gamma_{xz}')^2\right\}^{1/2} \tag{A-5}$$

and $\varepsilon_j' = \varepsilon_j^t$ - plastic strain.

With $\Delta\varepsilon_p$, ε_{et}, and ε_j^1 defined, the plastic strain components are computed from the Prandtl-Reuss flow rules.

$$\Delta\varepsilon_x^p = \frac{\Delta\varepsilon_p}{3\varepsilon_{et}} (2\varepsilon_x' - \varepsilon_y' - \varepsilon_z')$$

$$\Delta\varepsilon_y^p = \frac{\Delta\varepsilon_p}{3\varepsilon_{et}} (2\varepsilon_y' - \varepsilon_z' - \varepsilon_x')$$

$$\Delta\varepsilon_z^p = -\Delta\varepsilon_x^p - \Delta\varepsilon_y^p$$

$$\Delta\gamma_{xy}^p = \frac{\Delta\varepsilon_p}{3\varepsilon_{et}} \gamma_{xy}' \qquad \text{(A-6)}$$

$$\Delta\gamma_{yz}^p = \frac{\Delta\varepsilon_p}{3\varepsilon_{et}} \gamma_{yz}'$$

$$\Delta\gamma_{xz}^p = \frac{\Delta\varepsilon_p}{3\varepsilon_{et}} \gamma_{xz}'$$

If unloading is occurring, based on ε_{max} comparisons, then another equivalent, elastic, strain is computed.

$$\varepsilon_s = \frac{1}{\sqrt{2}(1+\nu)} \left\{ (\varepsilon_x^e - \varepsilon_y^e)^2 + (\varepsilon_y^e - \varepsilon_z^e)^2 + (\varepsilon_z^e - \varepsilon_x^e)^2 \right.$$

$$\left. + \frac{3}{2}(\gamma_{xy}^e)^2 + \frac{3}{2}(\gamma_{xz}^e)^2 + \frac{3}{2}(\gamma_{yz}^e)^2 \right\}^{1/2} \qquad \text{(A-7)}$$

where ε_i^e are elastic strains.

The equivalent stress during unloading is simply:

$$\sigma_{e,i} = E\, \varepsilon_s \,. \qquad \text{(A-8)}$$

If $\varepsilon_{max} < 0$, the unloading logic is complete. The conditions required for the negative ε_{max} are described later.

Since the equivalent stresses and strains used in the derivation are all positive, special provisions are made for evaluating load reversal during the unloading process. Specifically, the largest elastic normal strain component is compared to its corresponding plastic strain component. If they have opposite signs then the material is assumed to be unloading. To account for this, certain corrections to the strains are made. These include:

$$\varepsilon_{max} = - |\varepsilon_{max}|$$

Current origin shift strains = previous origin shift strains + 2 previous plastic strains

Current plastic strains = -previous plastic strains

$$\varepsilon_{e,i} = \varepsilon_{s,i} \qquad \text{(A-9)}$$

The effects of these adjustments is to convert the unloading into loading by shifting the origin and reversing the sign of the plastic strains. As was stated previously, the isotropic hardening used is an extension of one-dimensional plasticity. This manifests itself in the stress reversal evaluation and therefore the isotropic hardening is not recommended for general three-dimensional plasticity. The analyses made under the isotropic hardening rules have been shown to be consistent within themselves and with the kinematic hardening analyses, however.

KINEMATIC HARDENING

The classical bi-linear kinematic hardening used in ANSYS does not suffer the reversed loading difficulties found in the isotropic hardening behavior analysis. This is because it is

not developed as an extension of a one-dimensional case.

For the kinematic hardening, the plastic strain increment is defined differently. Specifically, the ϵ_{et} (eqn. A-5) term is defined in terms of $\epsilon_j' - \epsilon_j^{sh}$ instead of ϵ_j' and the yield stress is used instead of $\sigma_{e,i}$. The strain ϵ_j^{sh} is defined such that $E\epsilon_j^{sh}$ equals the increase in stress above the yield stress. In addition, the term $(d\sigma_e/d\epsilon_p)_{i-1}$ is defined as E(S)/1-S, where (S)E is the slope of the second line on part of the input bilinear stress-strain curves. When the computed value of $\Delta\epsilon_p$ (eqn. C-4) is greater than zero, yielding is occurring. Otherwise, unloading is occurring. A specific example given in reference 14 for the various strain calculations is:

$$(\epsilon_x^e)_i = (\epsilon_x')_i - \Delta\epsilon_x^p$$

$$(\epsilon_x^{pl})_i = (\epsilon_x^{pl})_{i-1} + \Delta\epsilon_x^p \qquad \text{(A-10)}$$

$$(\epsilon_x^{sh})_i = (\epsilon_x^{sh})_{i-1} + \Delta\epsilon_x^p \frac{2(1+\nu)}{2} \frac{S}{1-S}$$

The term $E\epsilon_j^{sh}$ is the amount that the yield surface is shifted within the stress space, in the j-direction. Since the relations do not use the equivalent stresses or strains for evaluating the plasticity effects, reversed loading behavior is handled directly and adjustments required for isotropic hardening are not needed.

Table 1. Elastic Constants (Room Temperature)

Elastic Constant	T-50 Graphite Fiber	2024-T4 Al Matrix
E_A (GPa)	388.2	72.4
E_T (GPa)	7.6	72.4
G_{AT} (GPa)	14.9	27.2
G_{TT} (GPa)	2.6	27.2
ν_{AT}	0.41	0.33
ν_{TT}	0.45	0.33
α_A m/m/°C	-0.68×10^{-6}	22.5×10^{-6}
α_T m/m/°C	9.74×10^{-6}	22.5×10^{-6}

A = Axial (Longitudinal)

T = Transverse

Table 2. Elastic Results (Room Temperature)

Elastic Constant	CCA*	F.E.**	% Difference
E_T (GPa)	41.78	42.26	1.1
G_{TT} (GPa)	14.99	15.13	0.9
G_A (GPa)	22.87	23.20	1.6
ν_{TT}	0.394	0.396	0.5
ν_{AT}	0.338	0.340 +	0.6
α_A m/m/°C	6.36	6.36	0.0
α_T m/m/°C	25.65	25.69	0.2

A = Axial (Longitudinal)

T = Transverse

*Composite Cylinder Assemblage

**Finite Element

+Computed using E_A from Rule of Mixtures and F.E. Results

Table 3. Transverse Tension and Temperature, Isotropic Hardening

Load Path	ε_2 %	ε_3 %	ε_1 %
1-2-3	-0.205	-0.616	-0.074
1-4	-0.190	-0.619	-0.073
% Difference	7.6	0.5	1.4
1-5-6	0.373	-0.506	-0.010
1-7	0.336	-0.465	-0.030
% Difference	10.4	8.4	NA

Load Steps

1. Stress Free Temperature to Room Temperature
2. Room Temperature to 204°C
3. σ_2 - 0 to 113.8 MPa
4. Simultaneous σ_2 - 0 to 113.8 and Room Temperature to 204°C
5. σ_2 - 0 to 172.4 MPa
6. Room Temperature to 299°C
7. Simultaneous σ_2 - 0 to 172.4 MPa and Room Temperature to 299°C

Table 4. Transverse Compression and Temperature, Isotropic Hardening

Load Path	ε_2 %	ε_3 %	ε_1 %
1-2-3	-0.790	-0.382	0.008
1-4	-0.794	-0.371	-0.018
% Difference	0.5	2.9	NA

Load Steps

1. Stress Free Temperature to Room Temperature
2. Room Temperature to 204°C
3. σ_2 - 0 to -113.8 MPa
4. Simultaneous σ_2 - 0 to -113.8 and Room Temperature to 204°C

Table 5. Transverse Tension and Temperature, Kinematic Hardening

Load Path	ε_2 %	ε_3 %	ε_1 %
1-2-3	-0.201	-0.614	-0.079
1-4	-0.234	-0.616	-0.077
% Difference	15.2	0.3	2.6

Load Steps

1. Stress Free Temperature to Room Temperature
2. Room Temperature to 204°C
3. σ_2 - 0 to 113.8 MPa
4. Simultaneous σ_2 - 0 to 113.8 and Room Temperature to 204°C

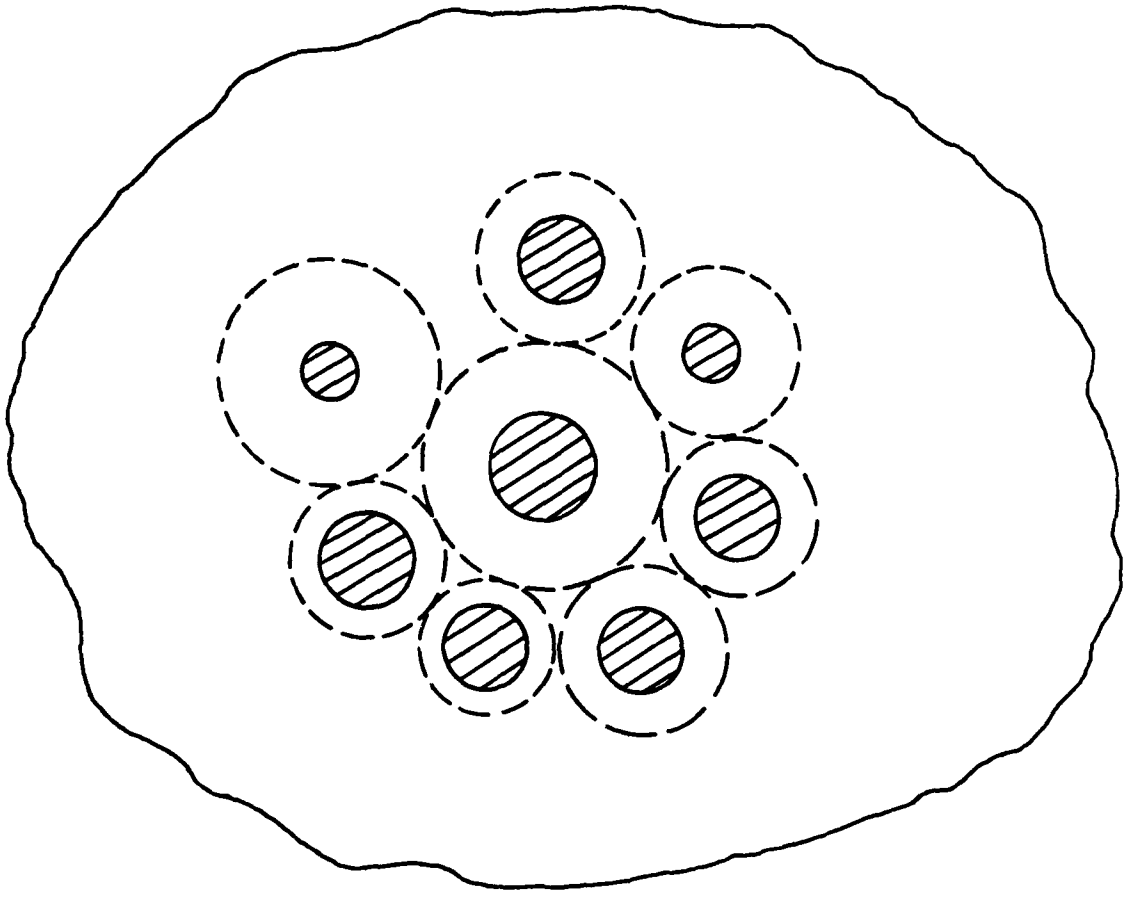

Figure 1. Composite Cylinder Assemblage

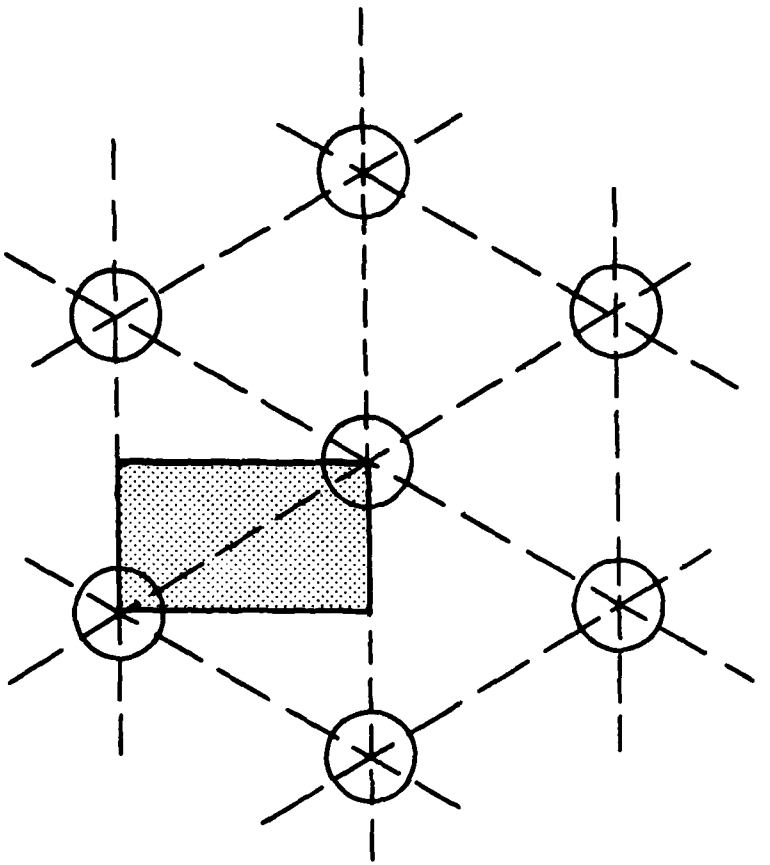

Figure 2. Hexagonal Fiber Array and Typical Repeating Element

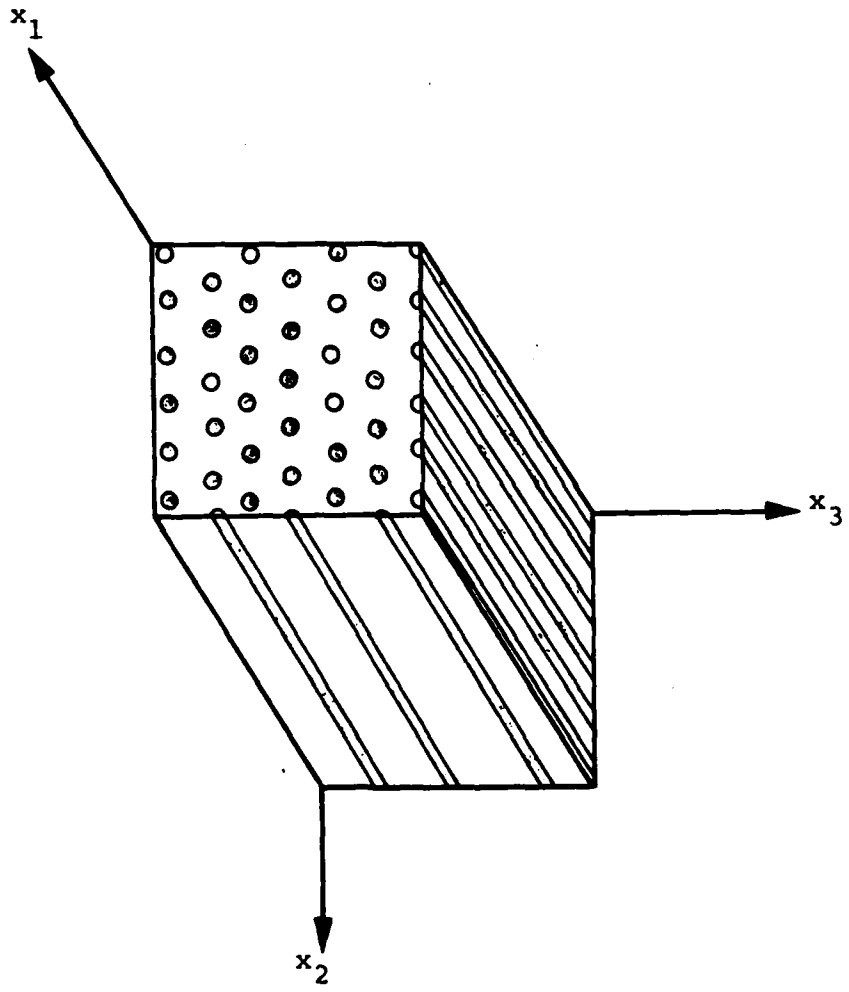

Figure 3. Prismatic Fiber Reinforced Specimen

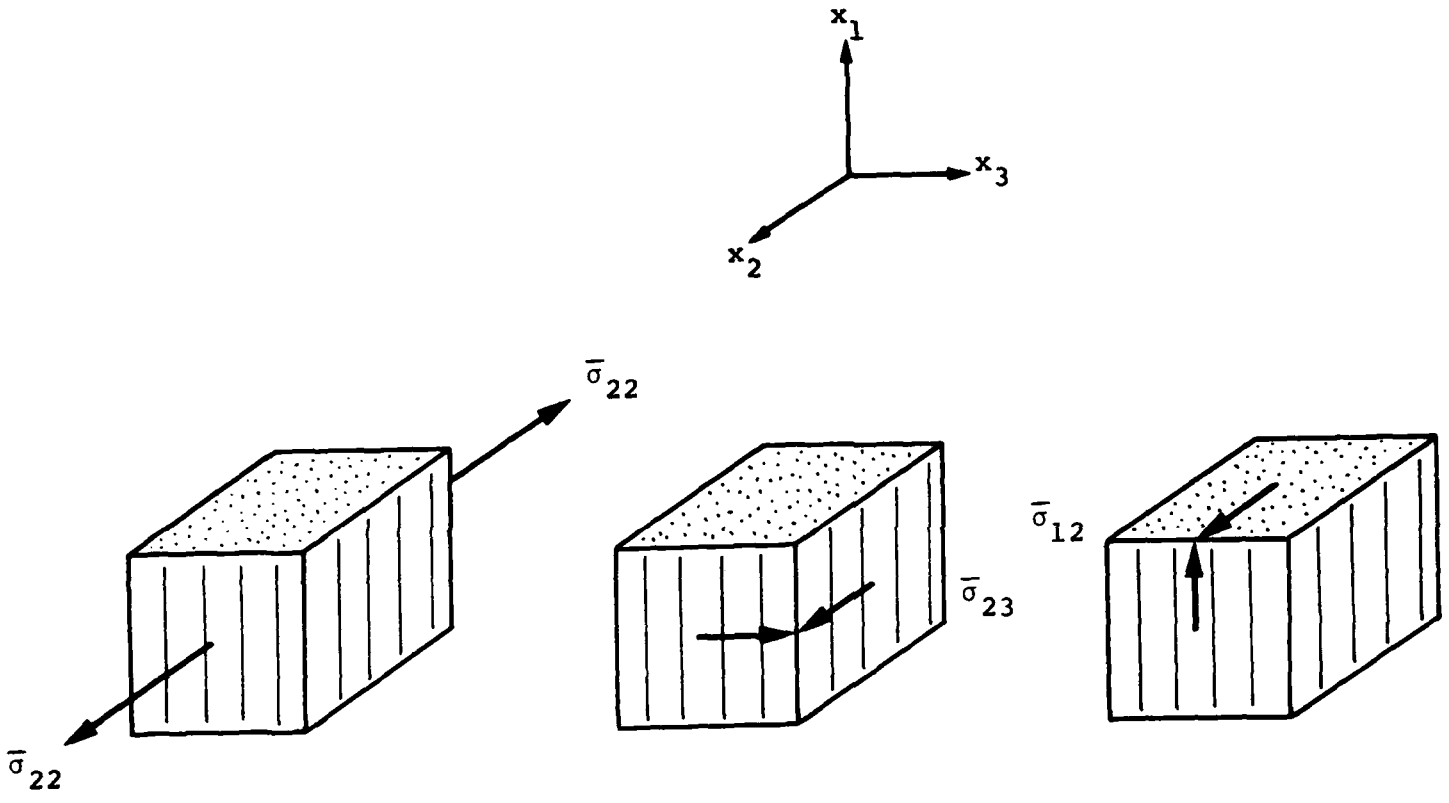

Figure 4. One-Dimensional Loadings

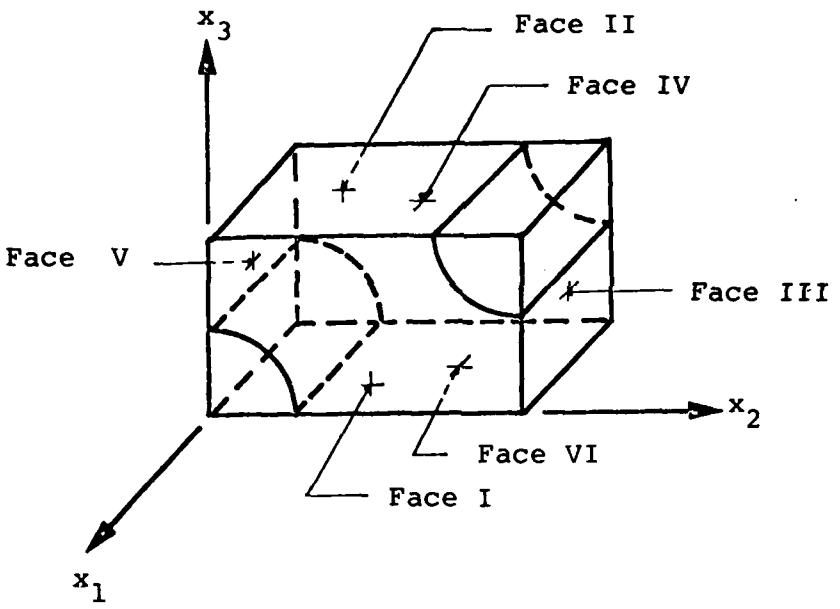

Figure 5. Repeating Element

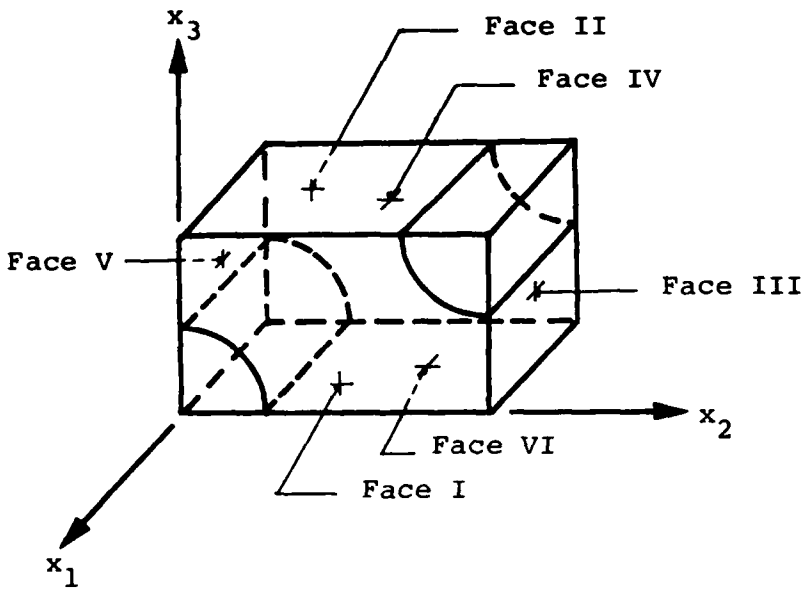

Transverse Shear

Face III Has Average Normal Force

$$F_2 = A_{III}\sigma$$

Face IV Has Average Normal Force

$$F_3 = -A_{IV}\sigma$$

Faces I & II Have Zero Average Normal Force

Faces II, V, & VI Fixed in Normal Direction

Faces I, III, & IV Deflect Uniformly in Normal Direction

Figure 6. Element Boundary Conditions for Transverse Shear

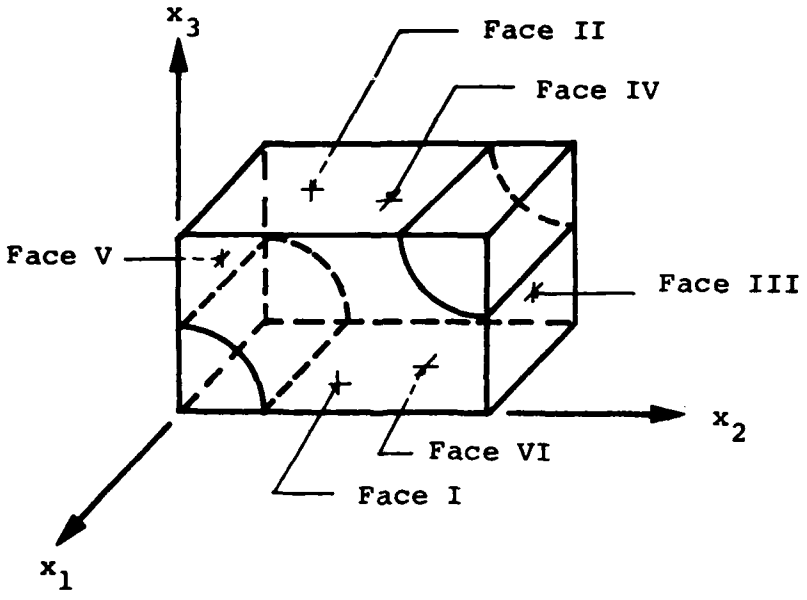

Free Thermal Expansion

Faces I-VI Have Zero Average Normal Force

Faces II, V, & VI Are Fixed in Normal Direction

Faces I, III, & IV Deflect Uniformly in Normal Direction

Transverse Extension (Compression)

Face III Has Average Normal Force

$$F_2 = A_{III}\sigma_2$$

Faces I, II, IV, & VI Have Zero Average Normal Force

Faces II, V, & VI Are Fixed in Normal Direction

Faces I, III, & IV Deflect Uniformly in Normal Direction

Figure 7. Element Boundary Conditions for Thermal Expansion and Transverse Load

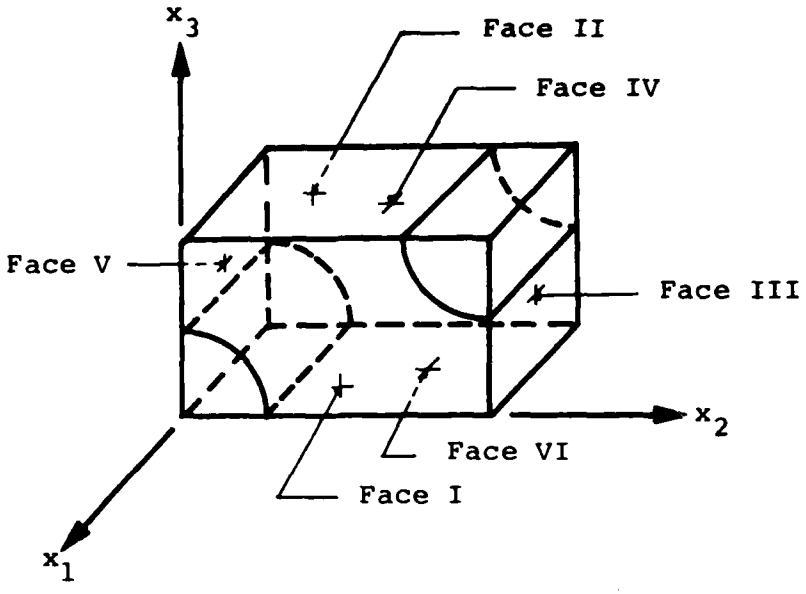

Axial Shear

Face I Has Shear Force

$F_2 = A_1\tau$

Face II is Fixed in x_2-Direction

$U_3 = 0$ Everywhere

Faces III-VI Are Fixed in x_1-Direction

U_2 is Linear in x_1

Figure 8. Element Boundary Conditions for Axial Shear

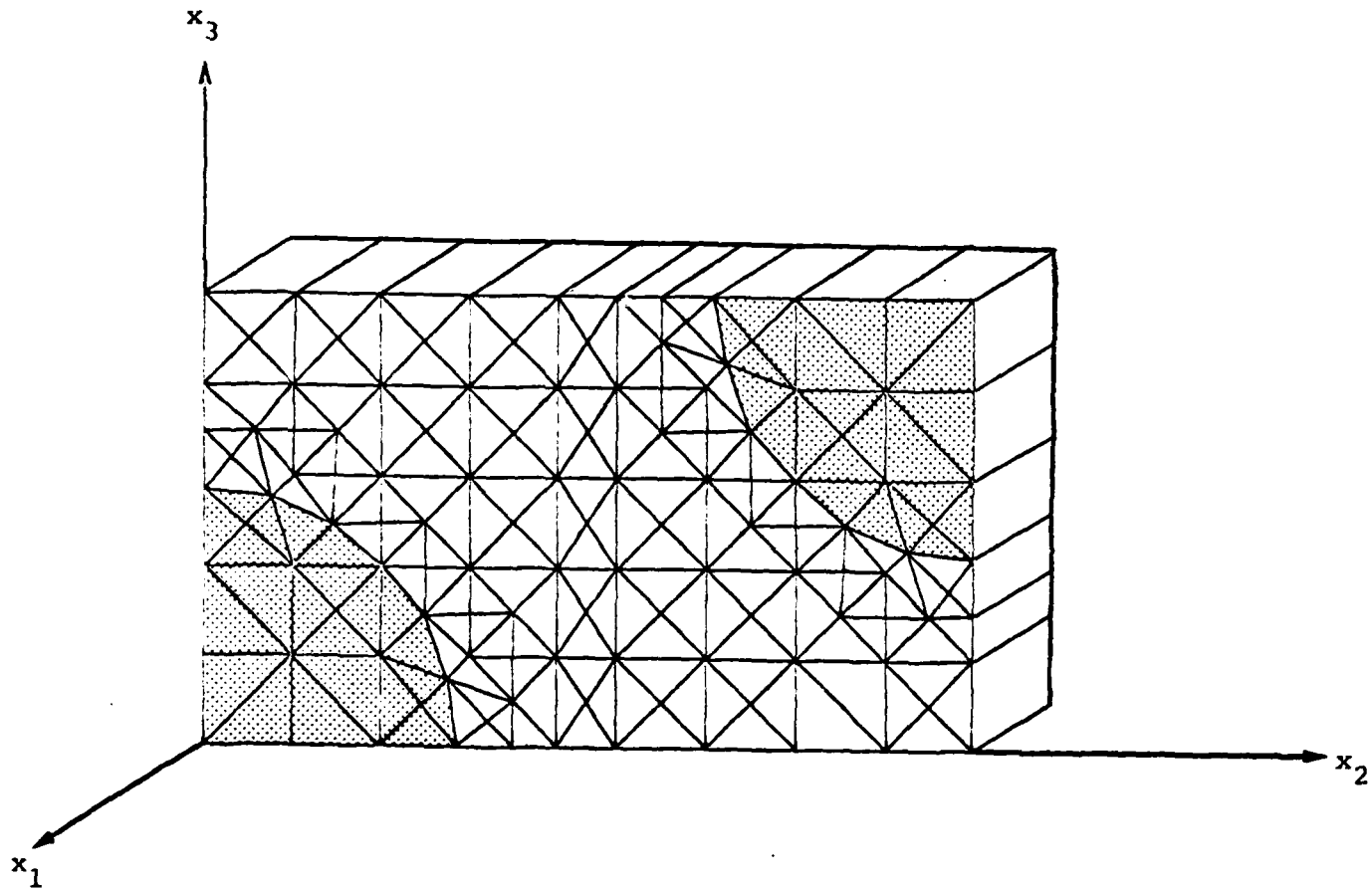

Figure 9. Finite Element Model

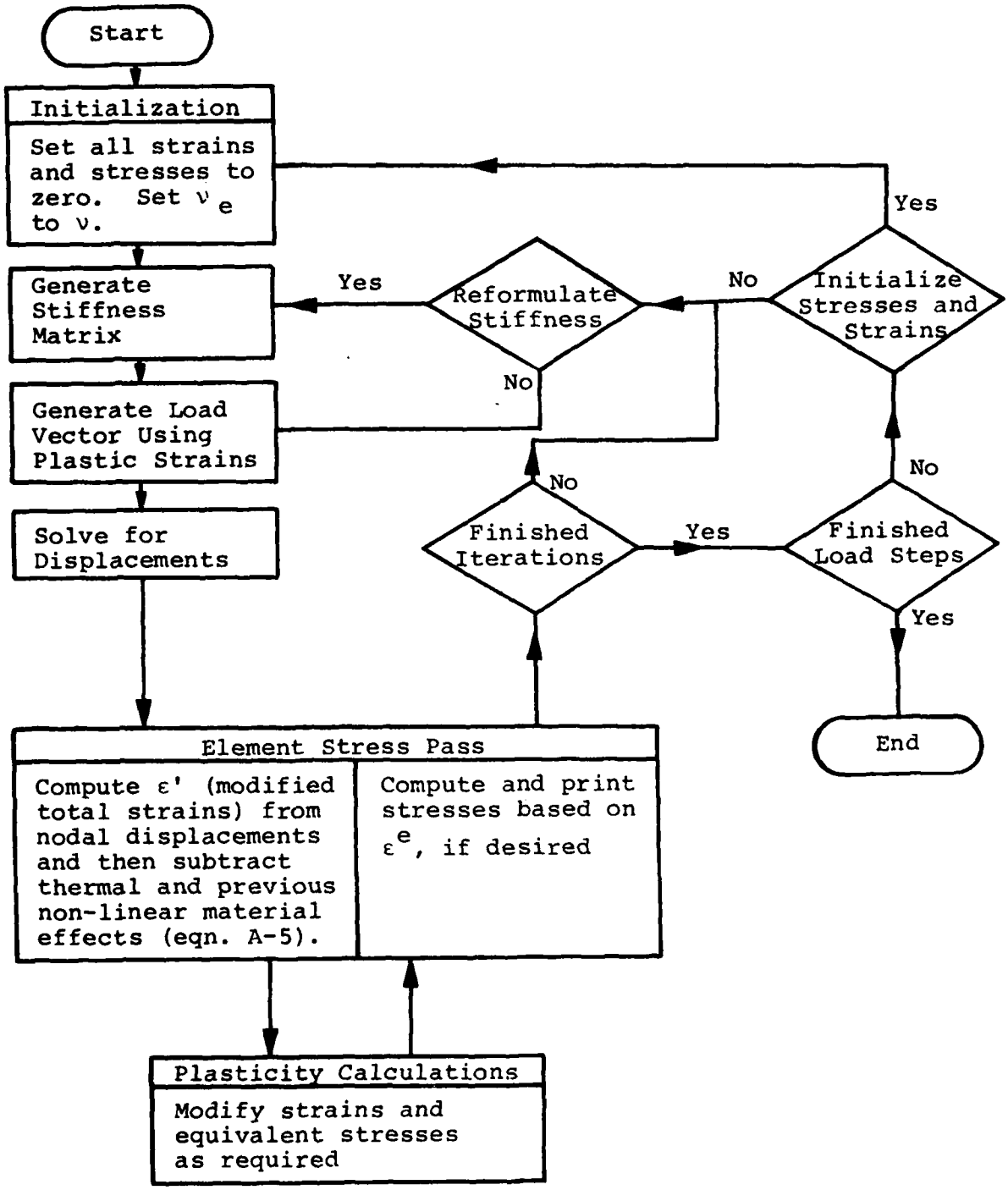

Figure 10. ANSYS Plasticity Procedure (After Swanson Analysis, Inc., ref. 14)

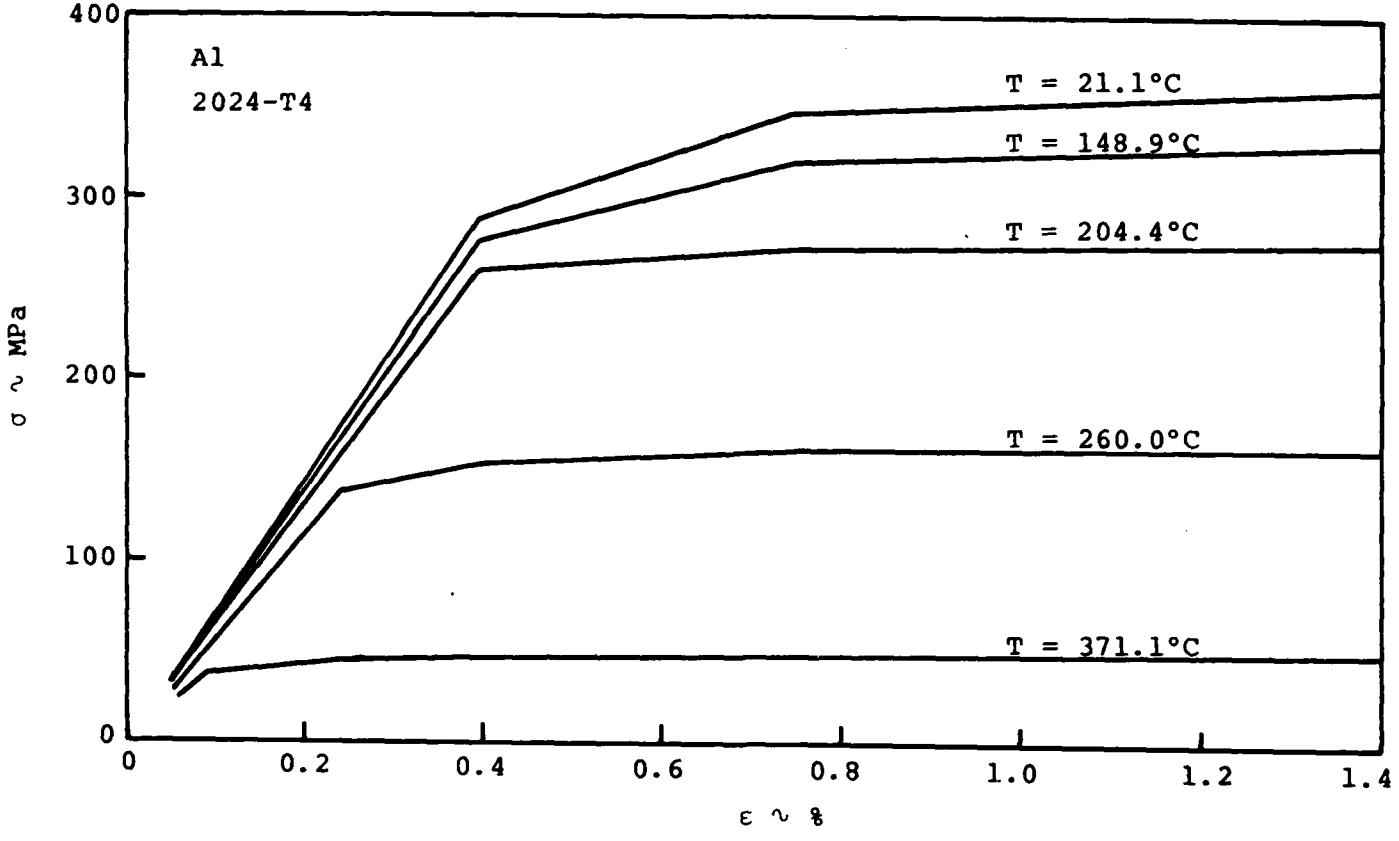

Figure 11. Input Matrix Properties, Isotropic Hardening

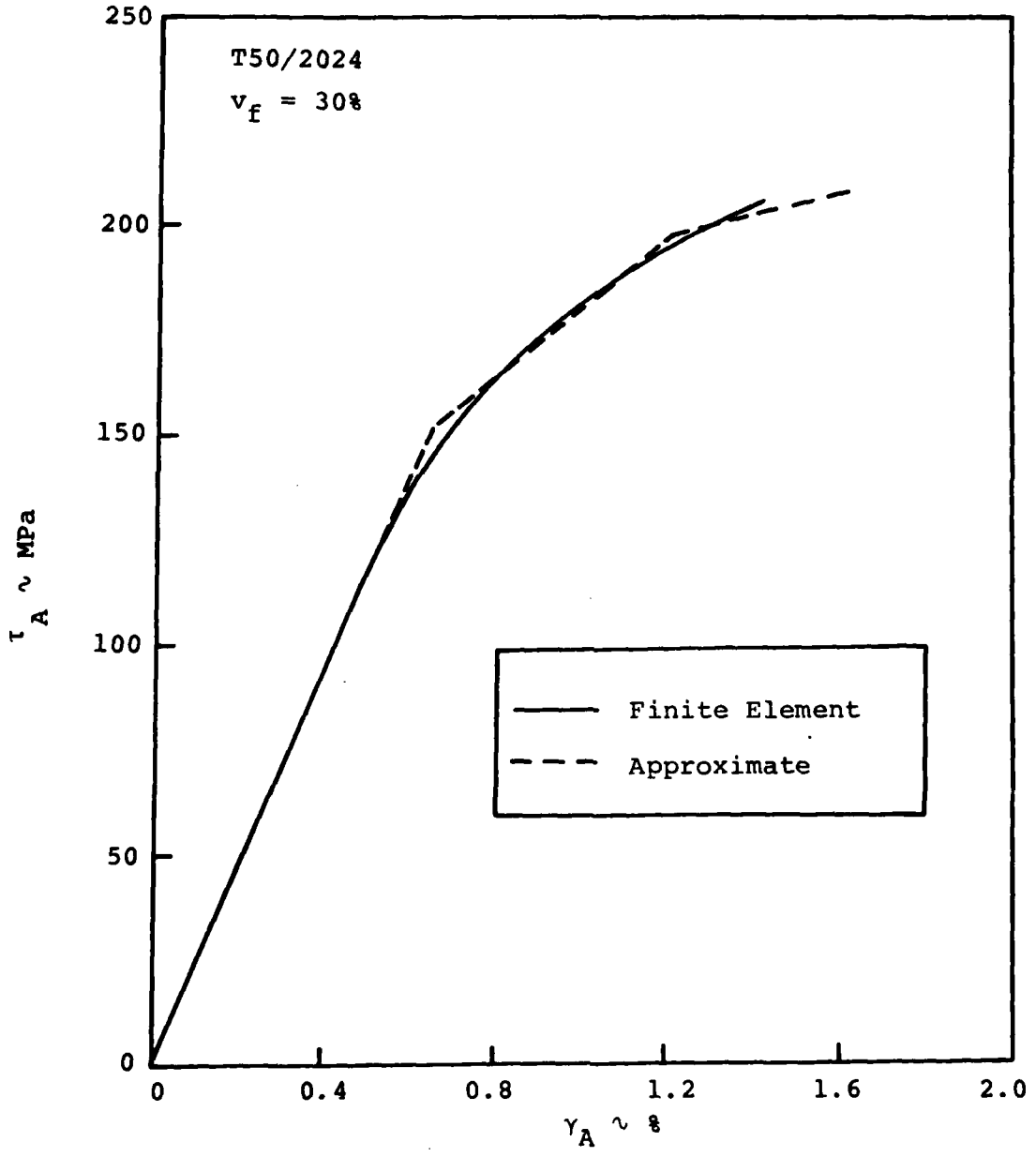

Figure 12. Axial Shear Stress-Strain Relation, Finite Element Solution, Hexagonal Array and Approximate Treatment

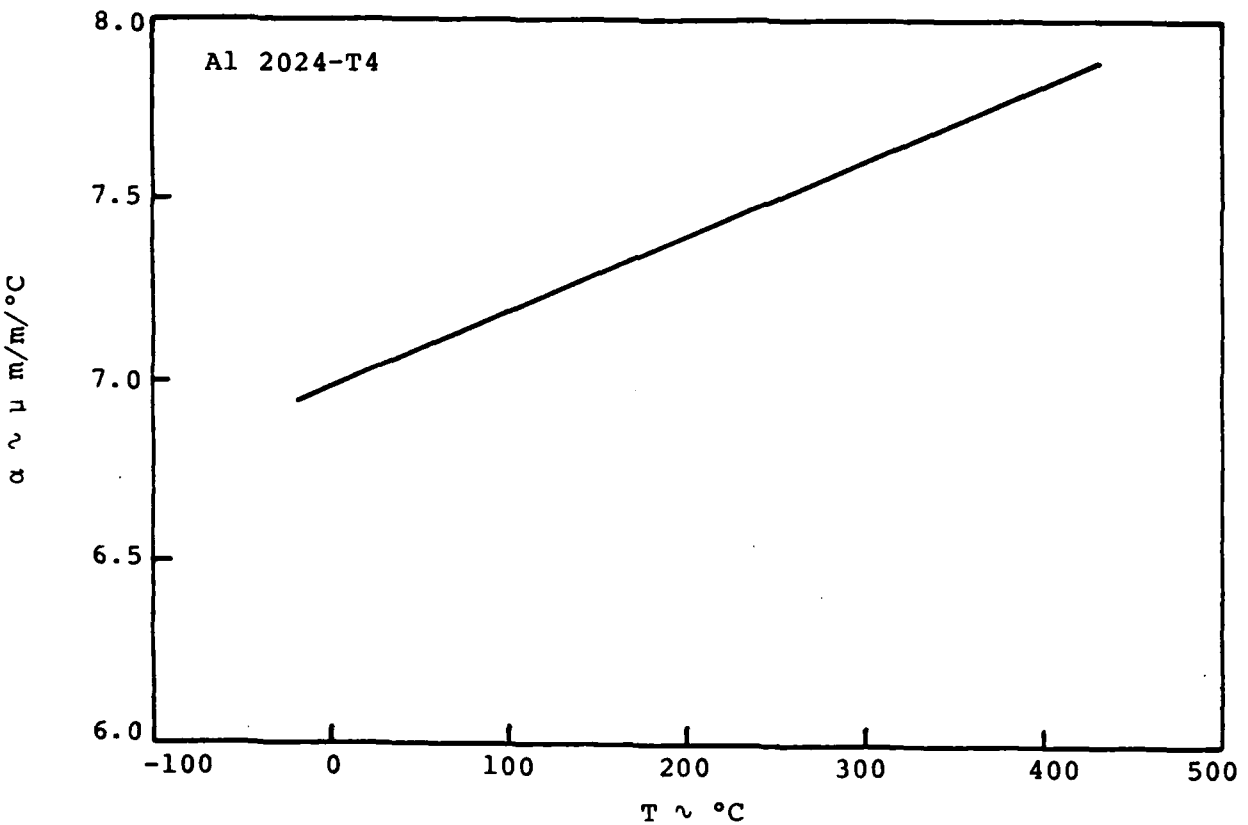

Figure 13. Coefficient of Thermal Expansion vs. Temperature of Aluminum Matrix

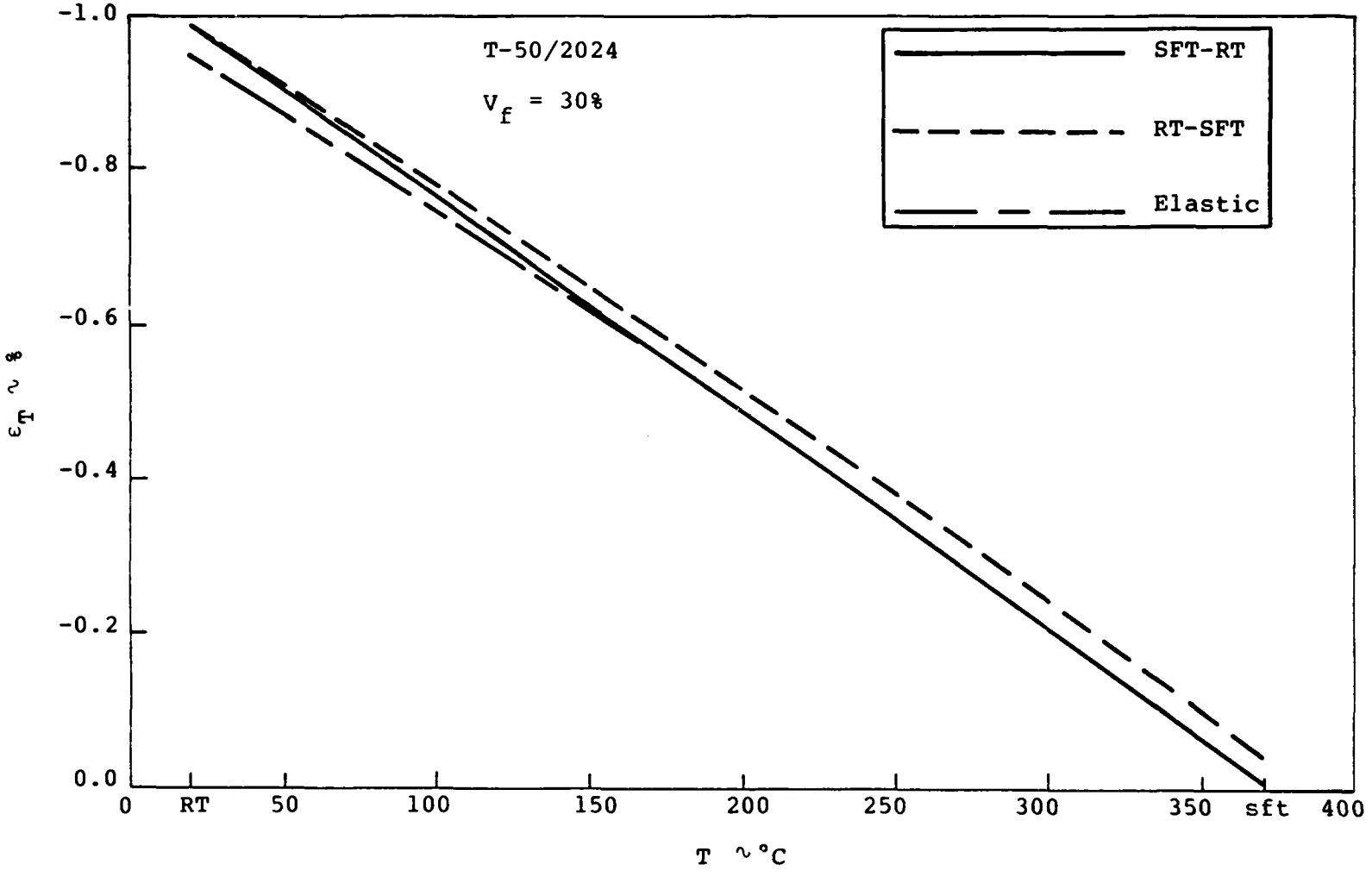

Figure 14. Transverse Thermal Expansion, Isotropic Hardening

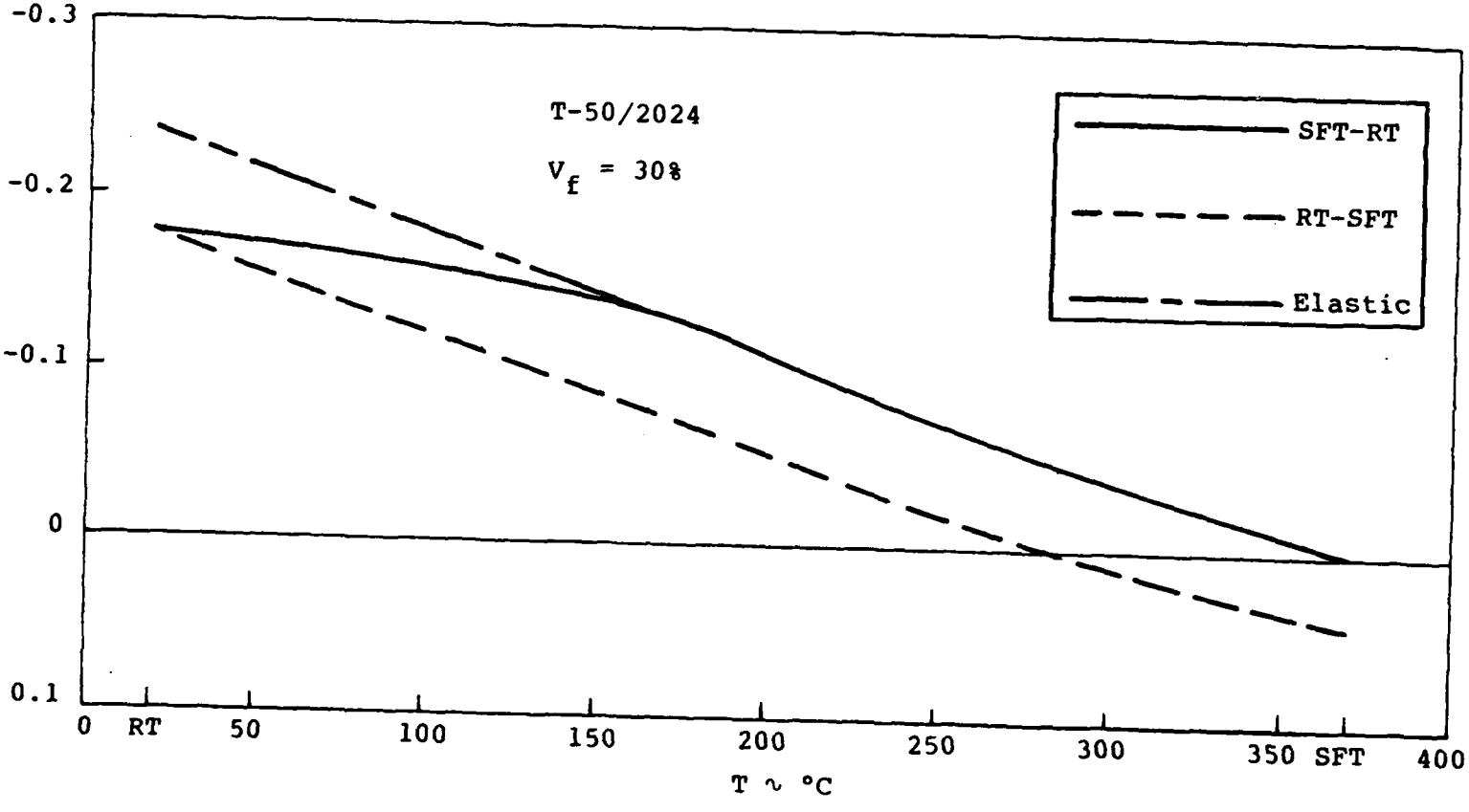

Figure 15. Axial Thermal Expansion, Isotropic Hardening

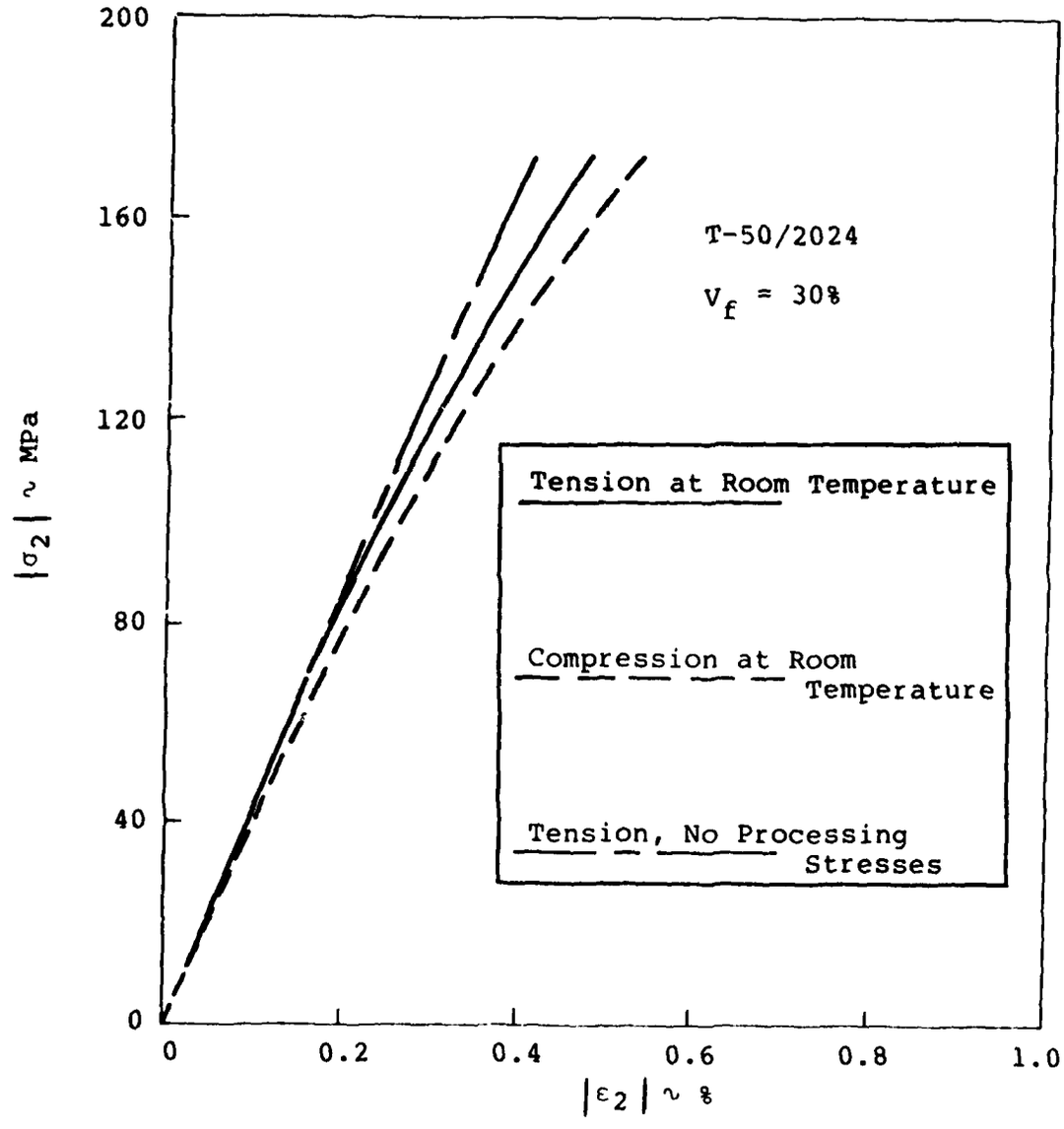

Figure 16. Transverse Stress-Strain Response, Isotropic Hardening

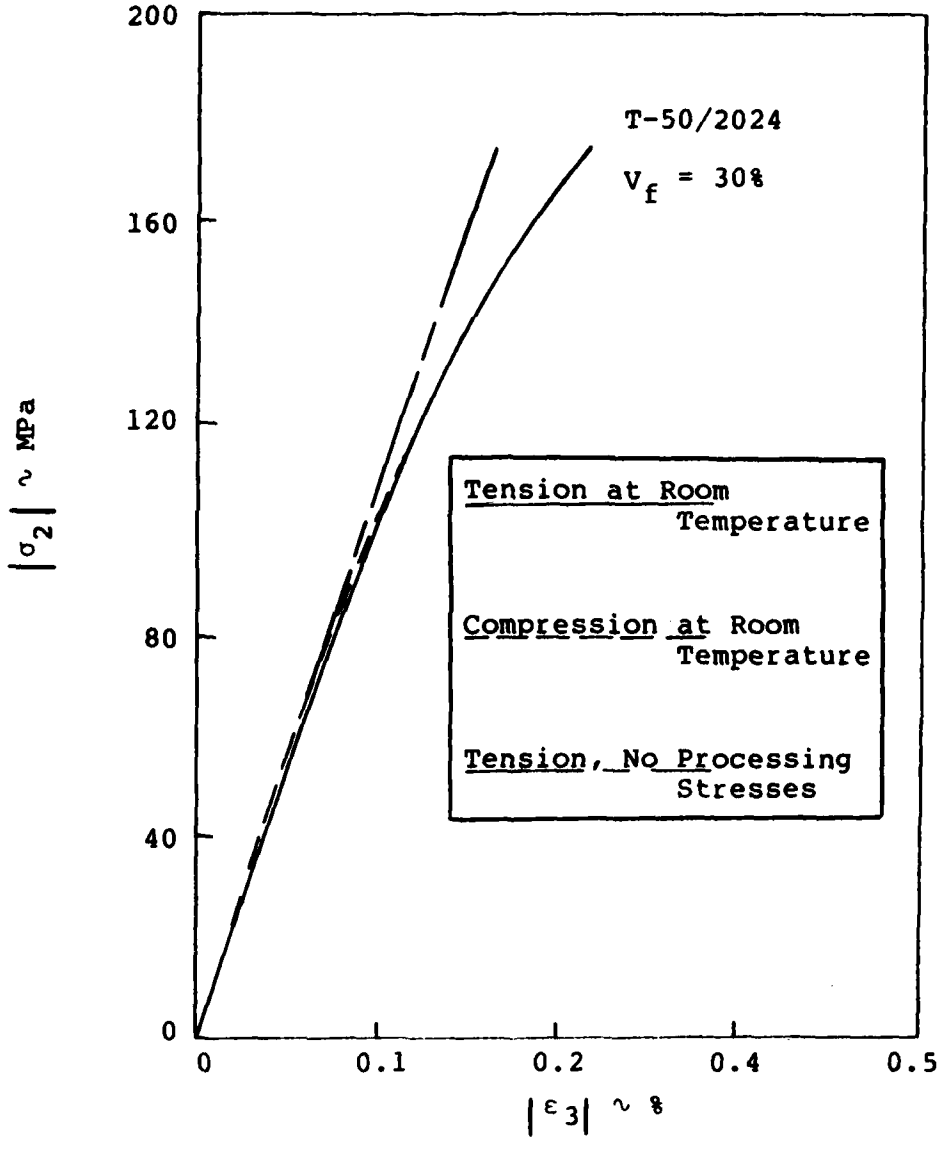

Figure 17. Transverse Normal Strain vs. Transverse Stress, Isotropic Hardening

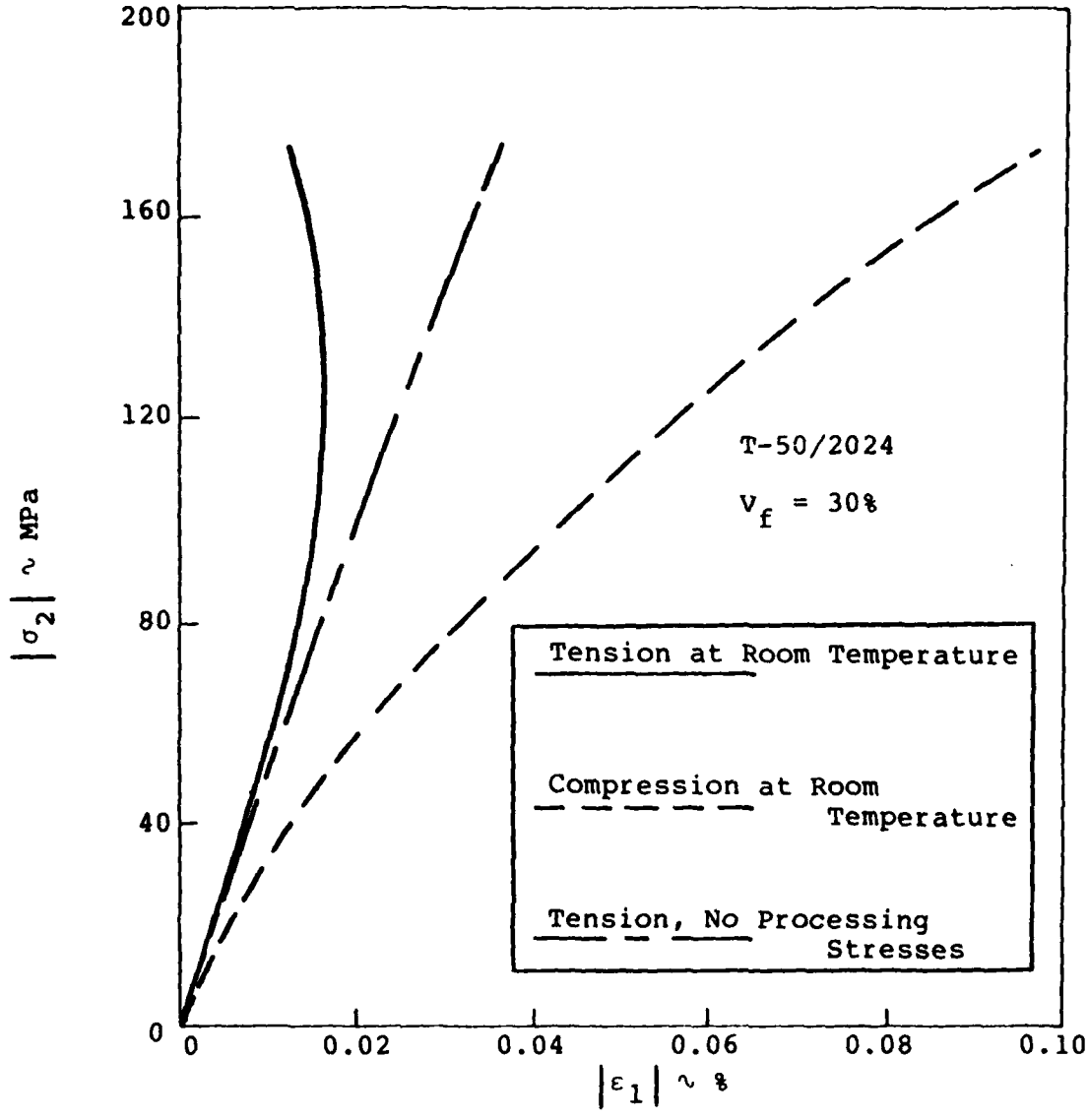

Figure 18. Axial Strain vs. Transverse Stress, Isotropic Hardening

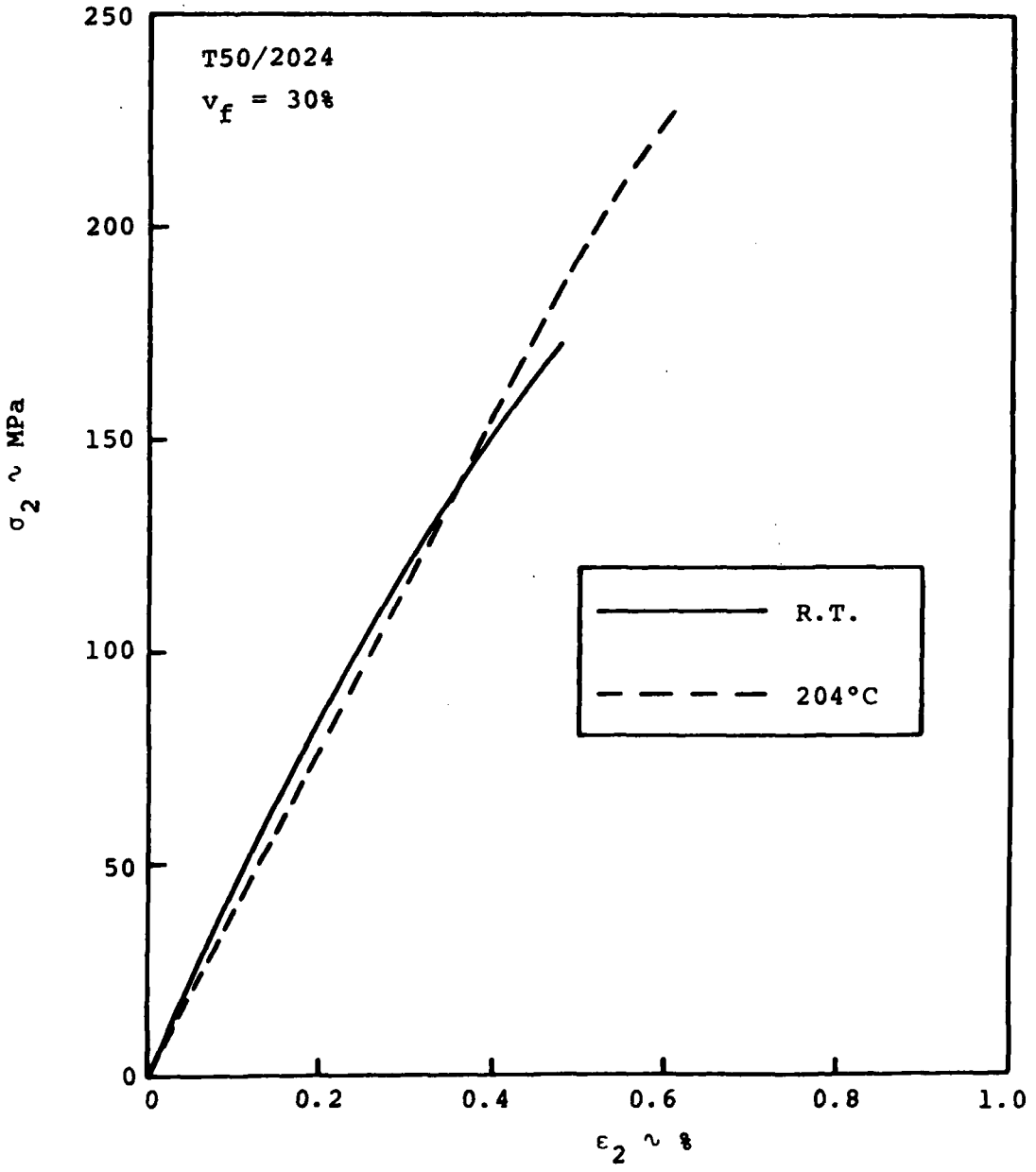

Figure 19. Transverse Tensile Stress-Strain Response at 204°C, Isotropic Hardening

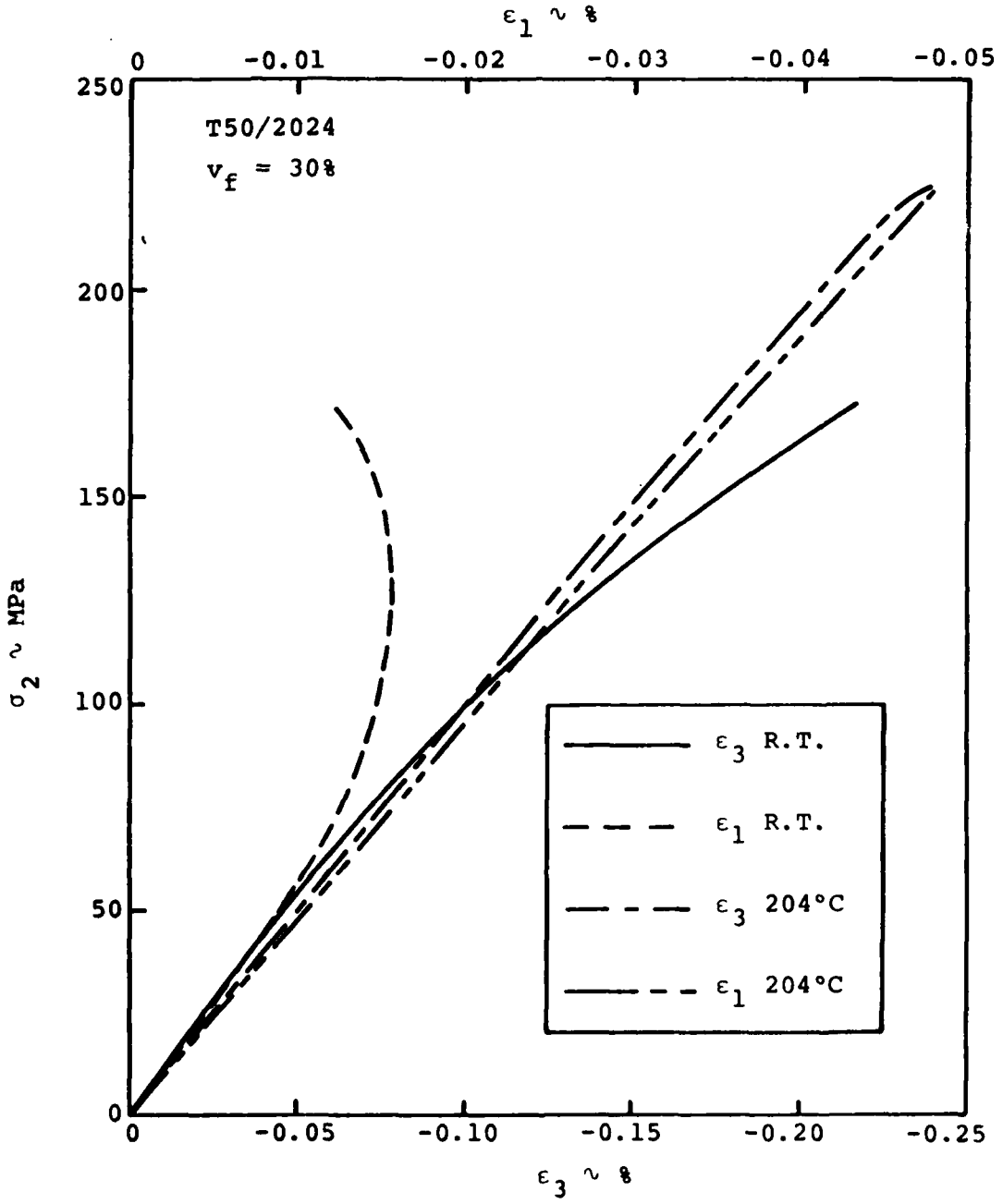

Figure 20. Transverse Normal and Axial Strain vs. Transverse Tensile Stress at 204°C, Isotropic Hardening

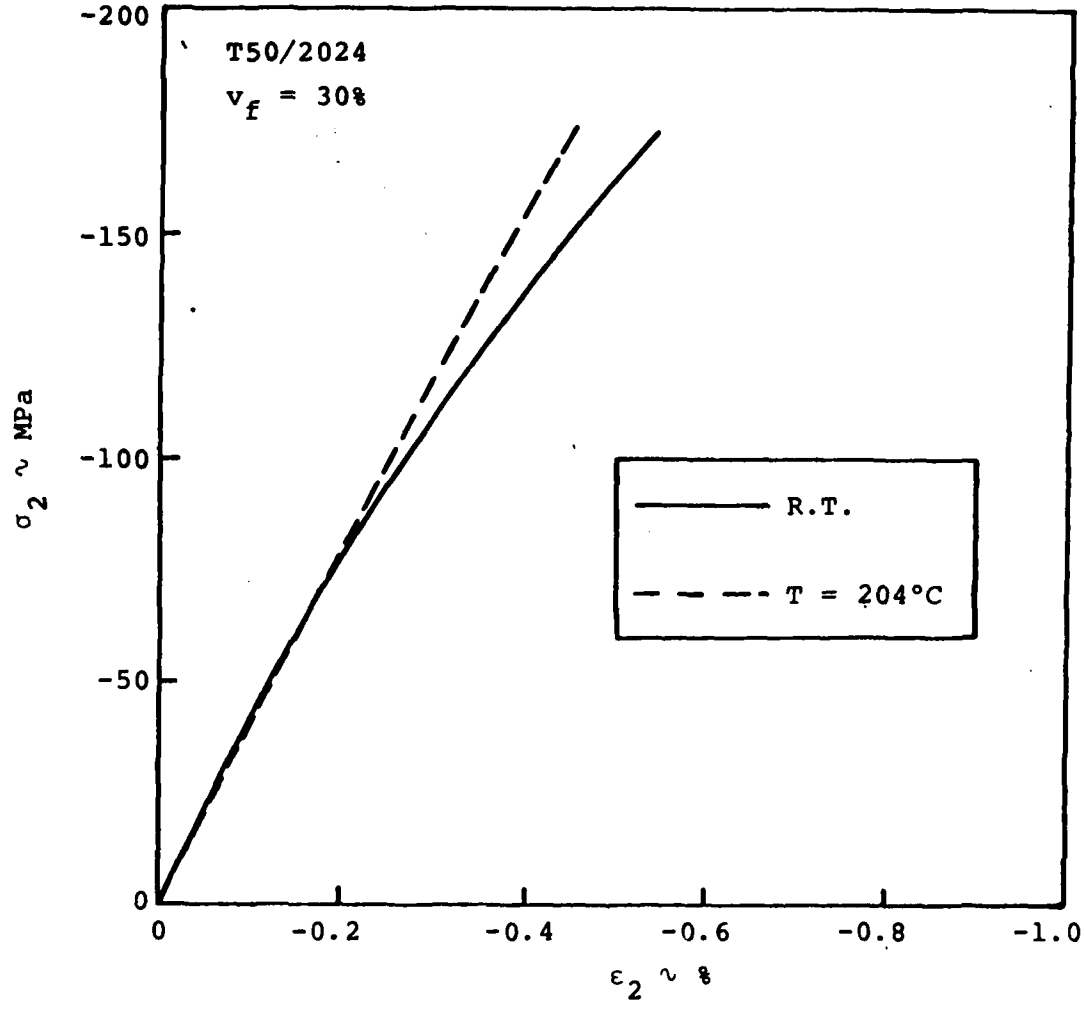

Figure 21. Transverse Compressive Stress-Strain Response at 204°C, Isotropic Hardening

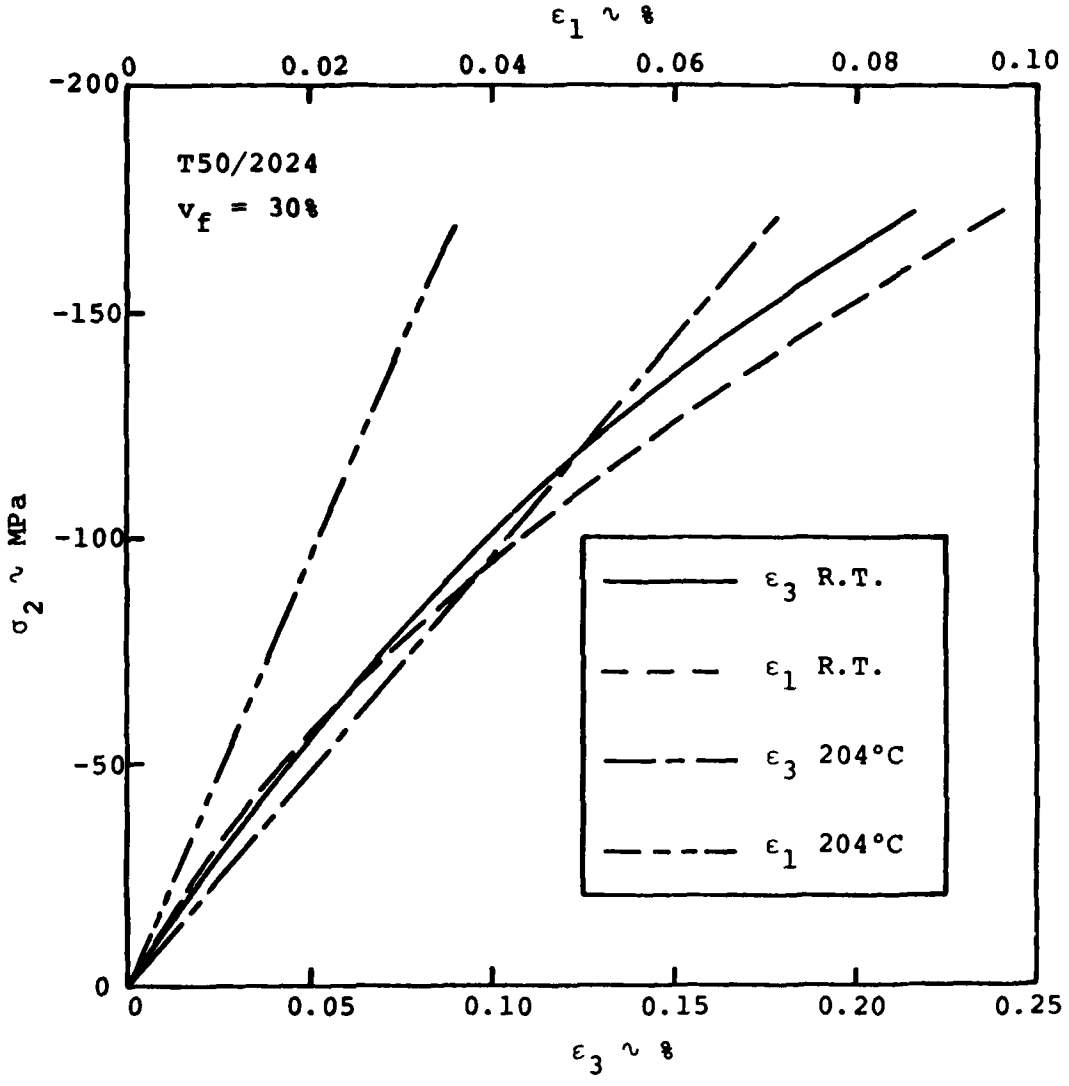

Figure 22. Transverse Normal and Axial Strain vs. Transverse Compressive Stress at 204°C, Isotropic Hardening

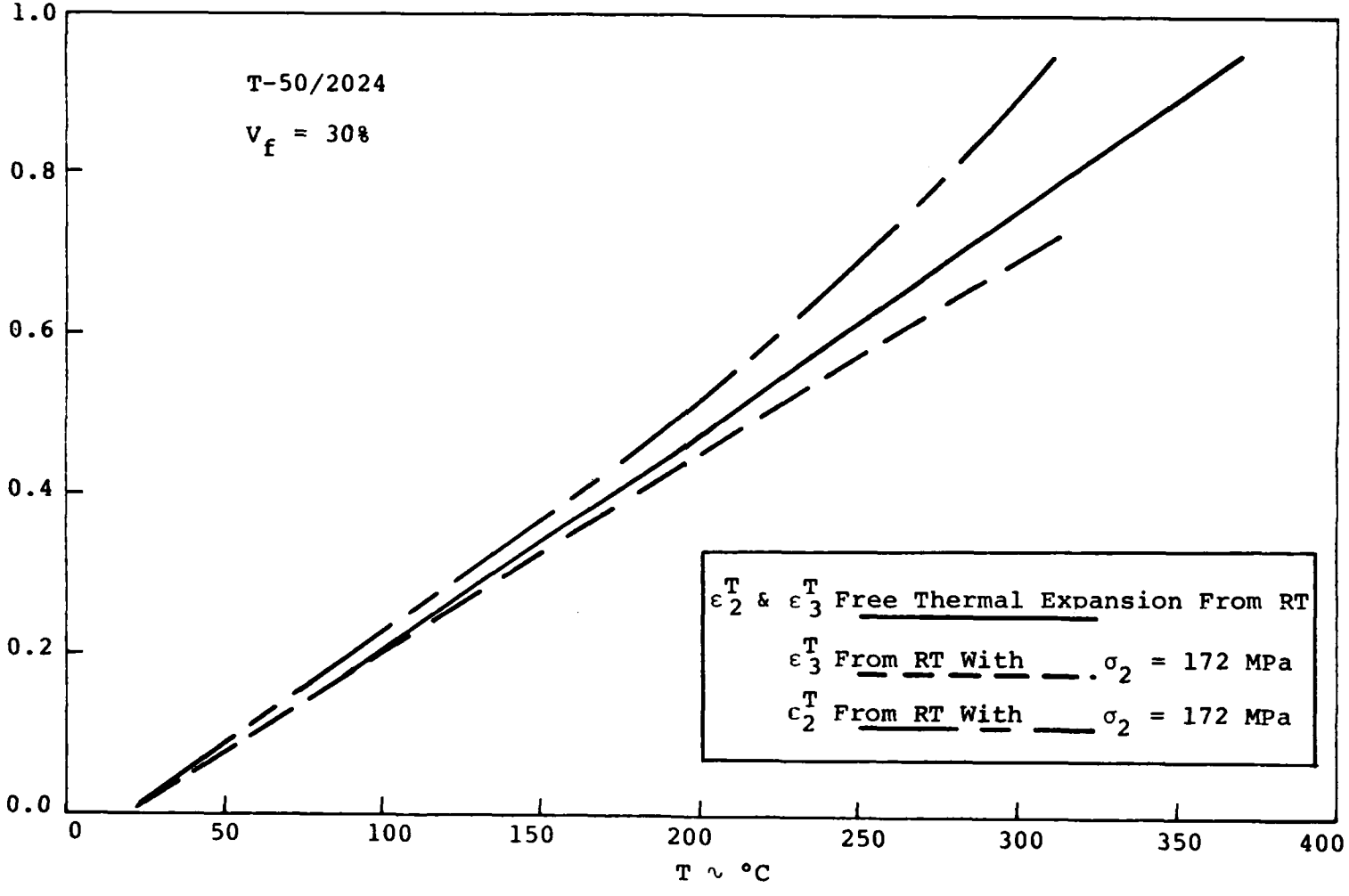

Figure 23. Effect of Applied Stress on Transverse Thermal Expansion, Isotropic Hardening

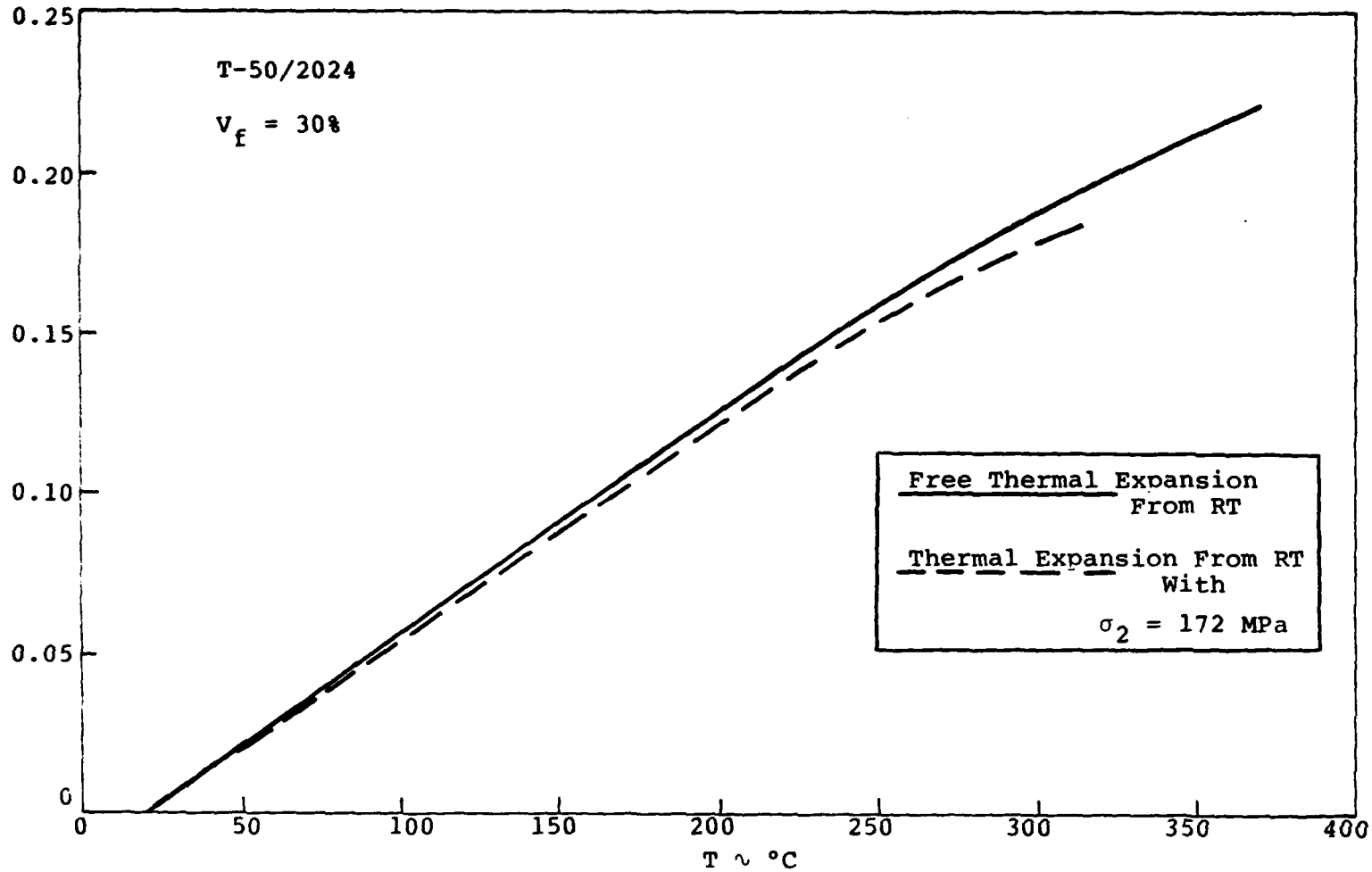

Figure 24. Effect of Applied Stress on Axial Thermal Expansion, Isotropic Hardening

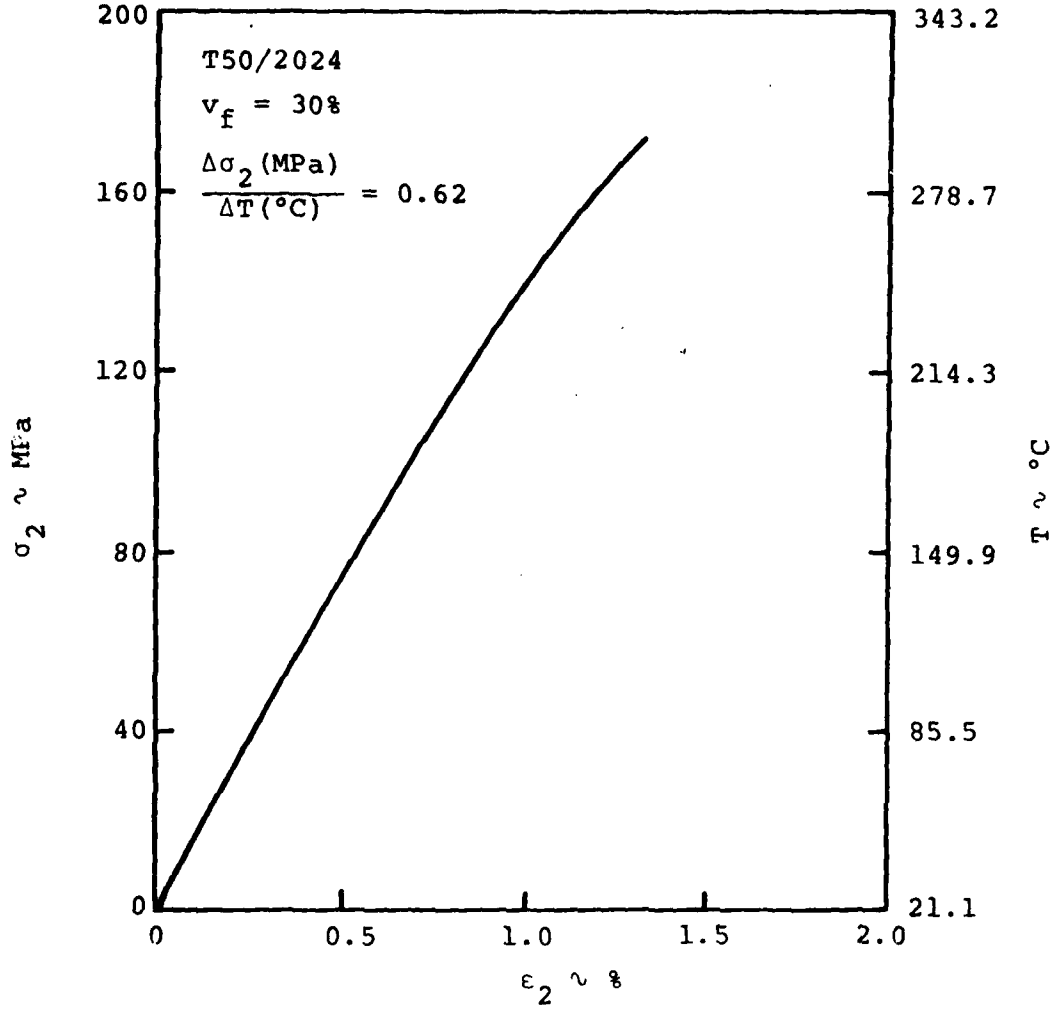

Figure 25. Proportional Simultaneous Variations of σ_2 and T From R.T., Isotropic Hardening

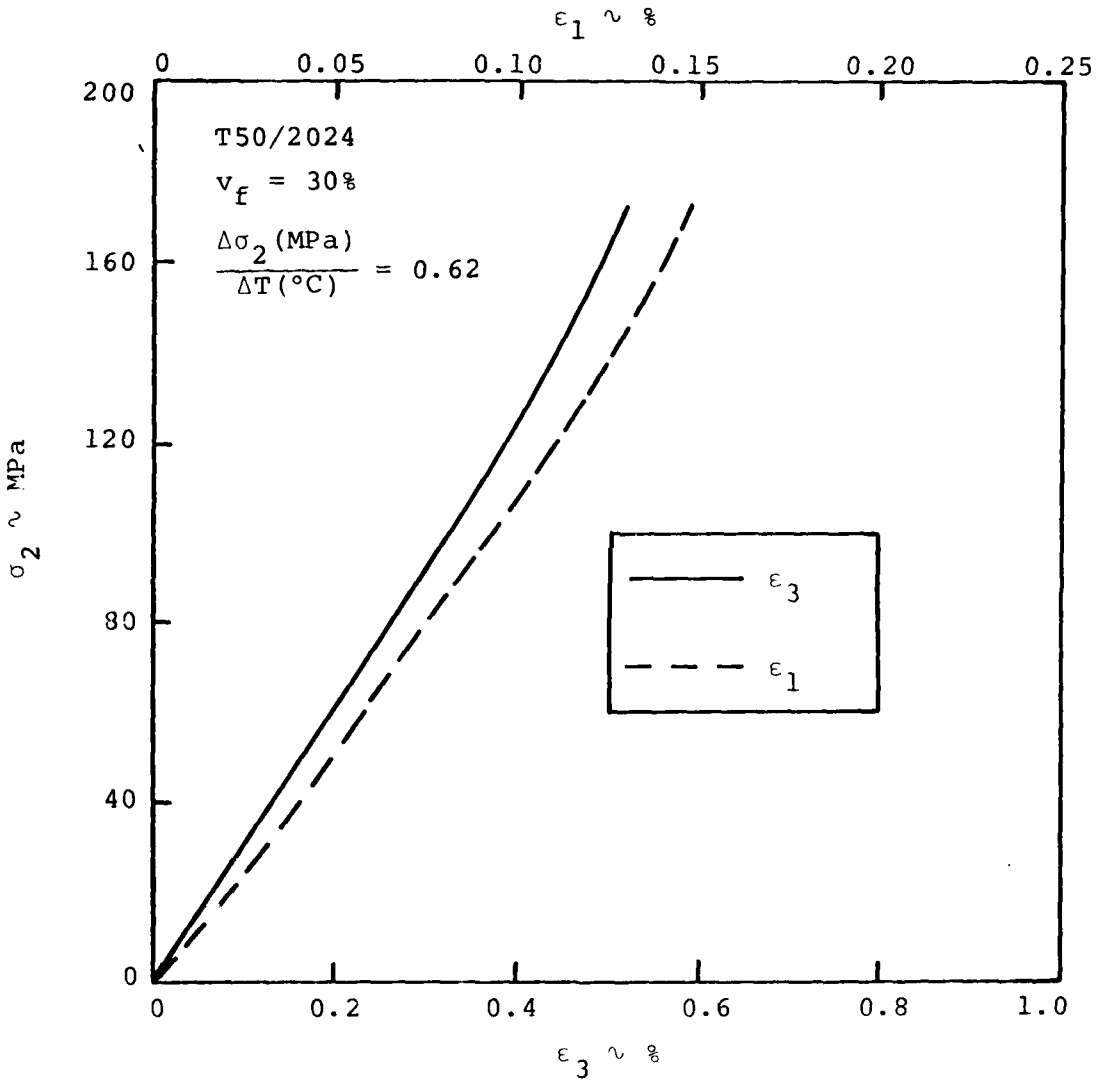

Figure 26. Proportional Simultaneous Variations of σ_2 and T From R.T., Poisson Induced Strains, Isotropic Hardening

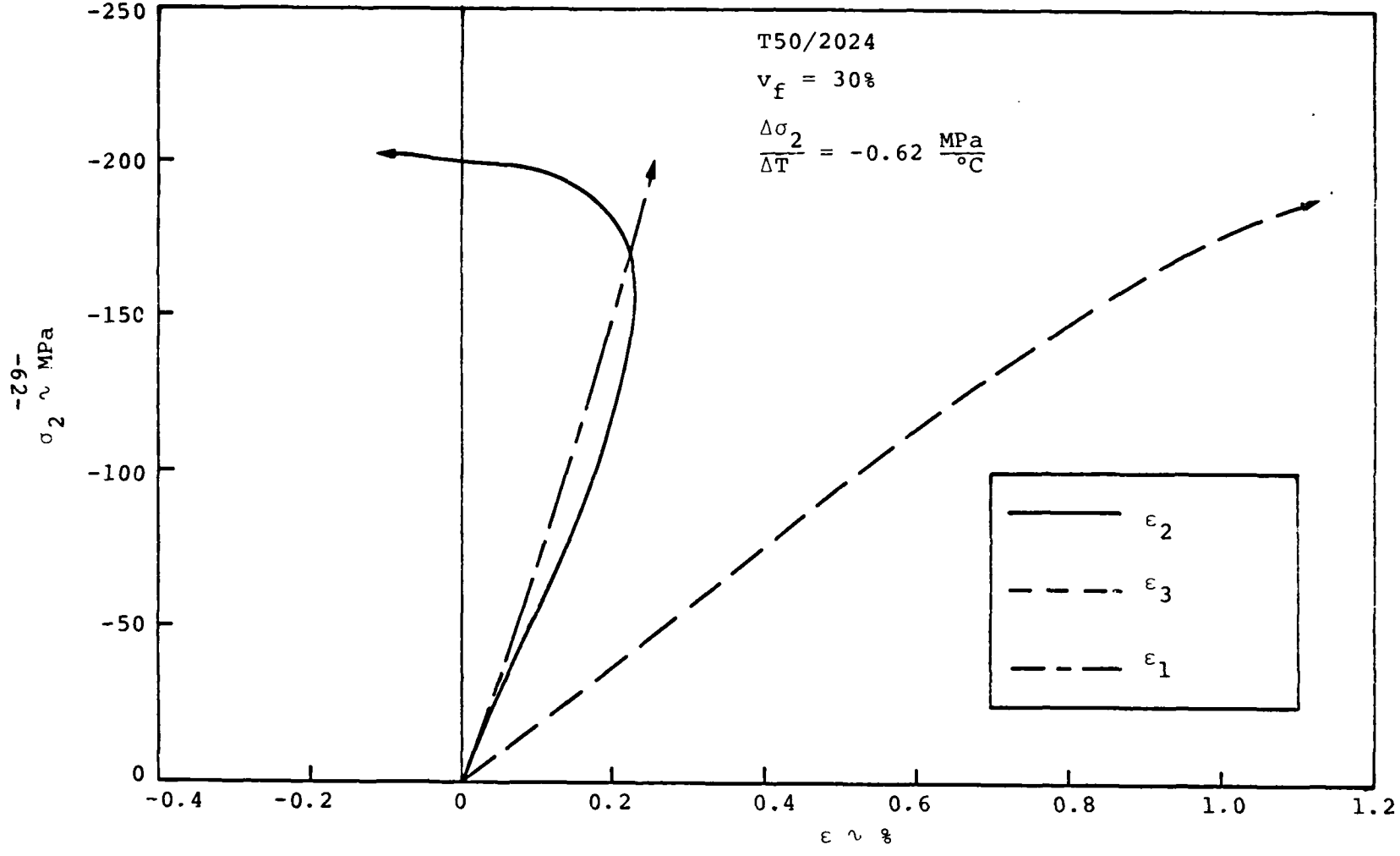

Figure 27. Proportional Simultaneous Transverse Compression and Temperature from R.T., Isotropic Hardening

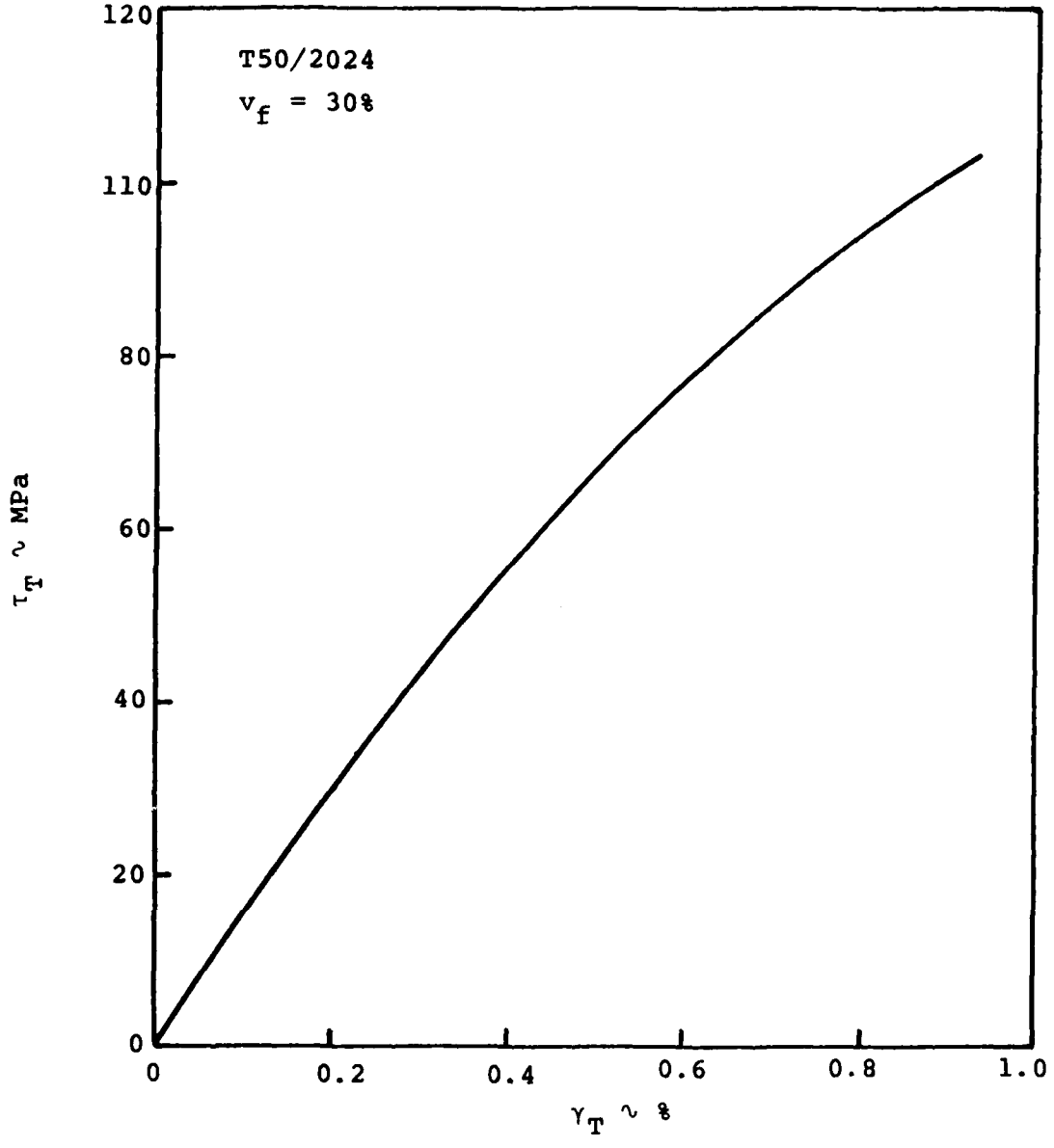

Figure 28. Transverse Shear Stress-Strain Response at R.T., Isotropic Hardening

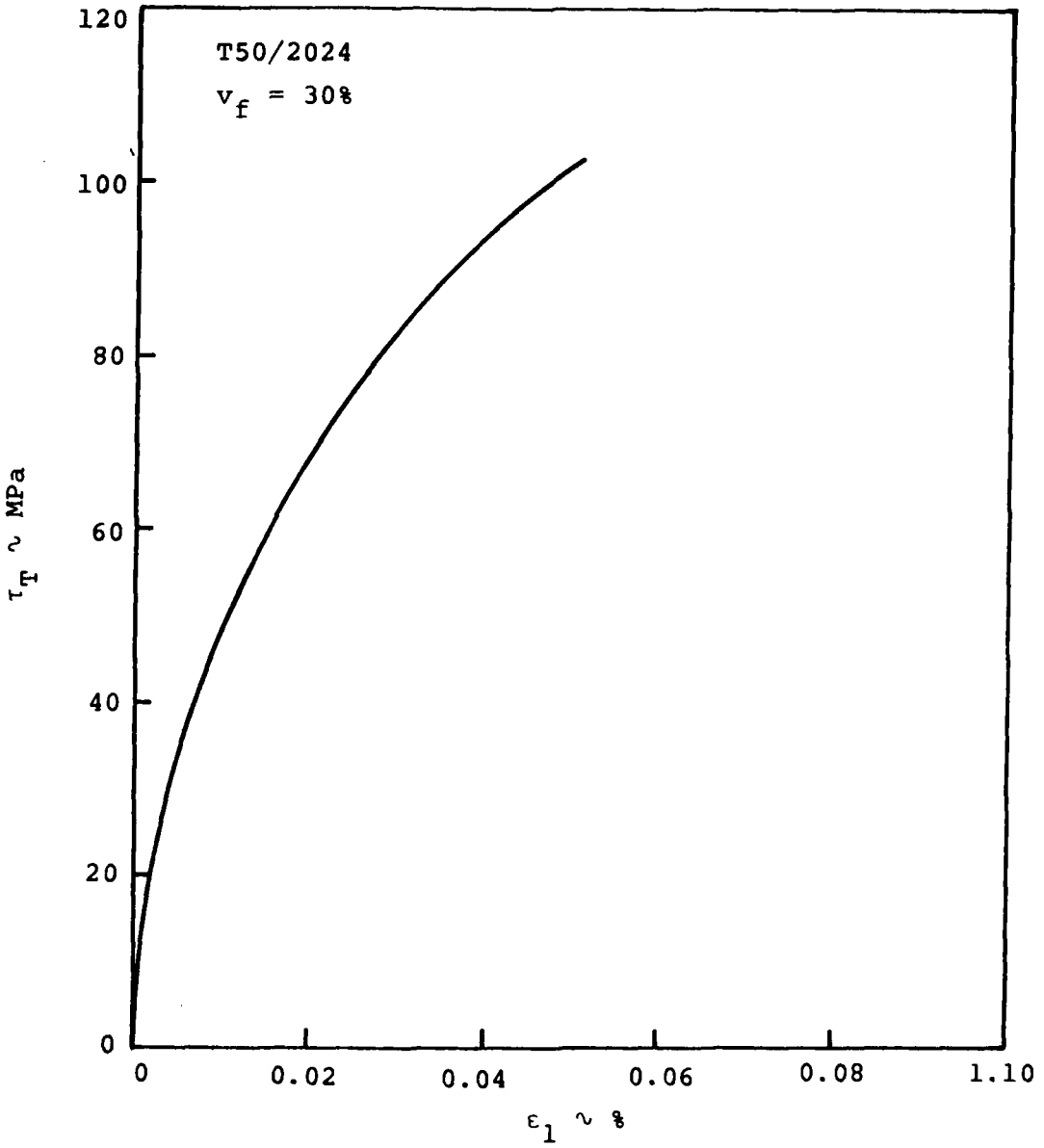

Figure 29. Axial Strain vs. Transverse Shear Stress at R.T., Isotropic Hardening

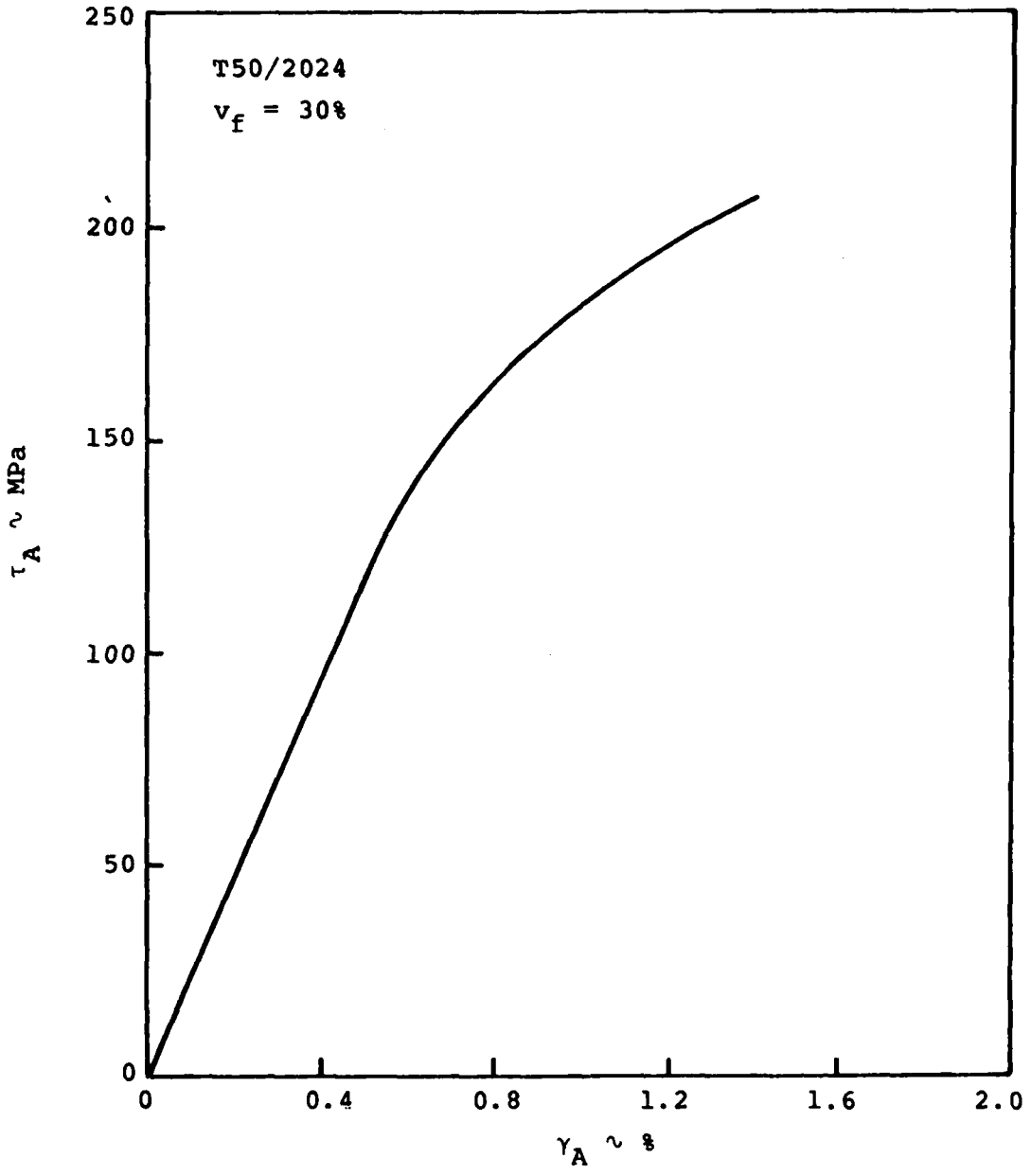

Figure 30. Axial Shear Stress-Strain Response With No Processing Stresses

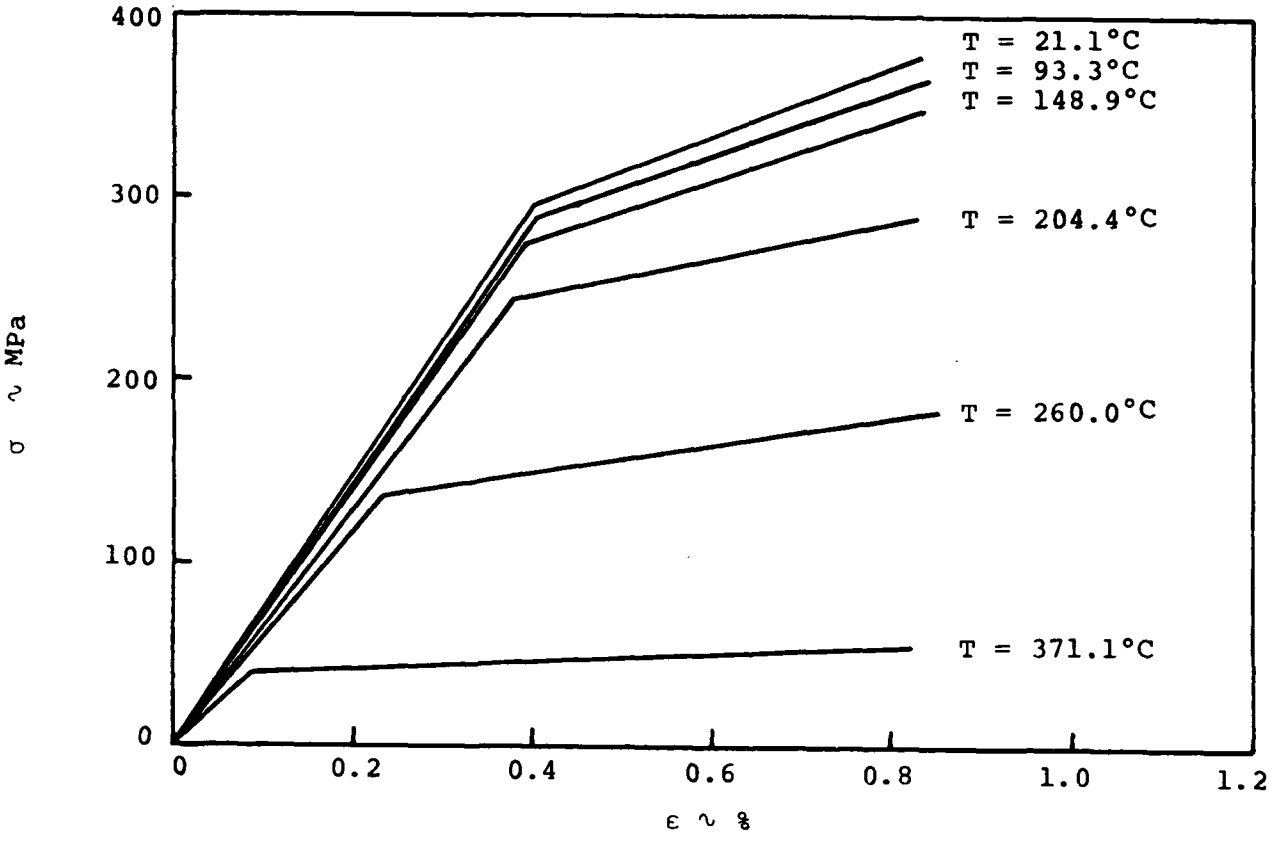

Figure 31. Input Matrix Properties, Kinematic Hardening

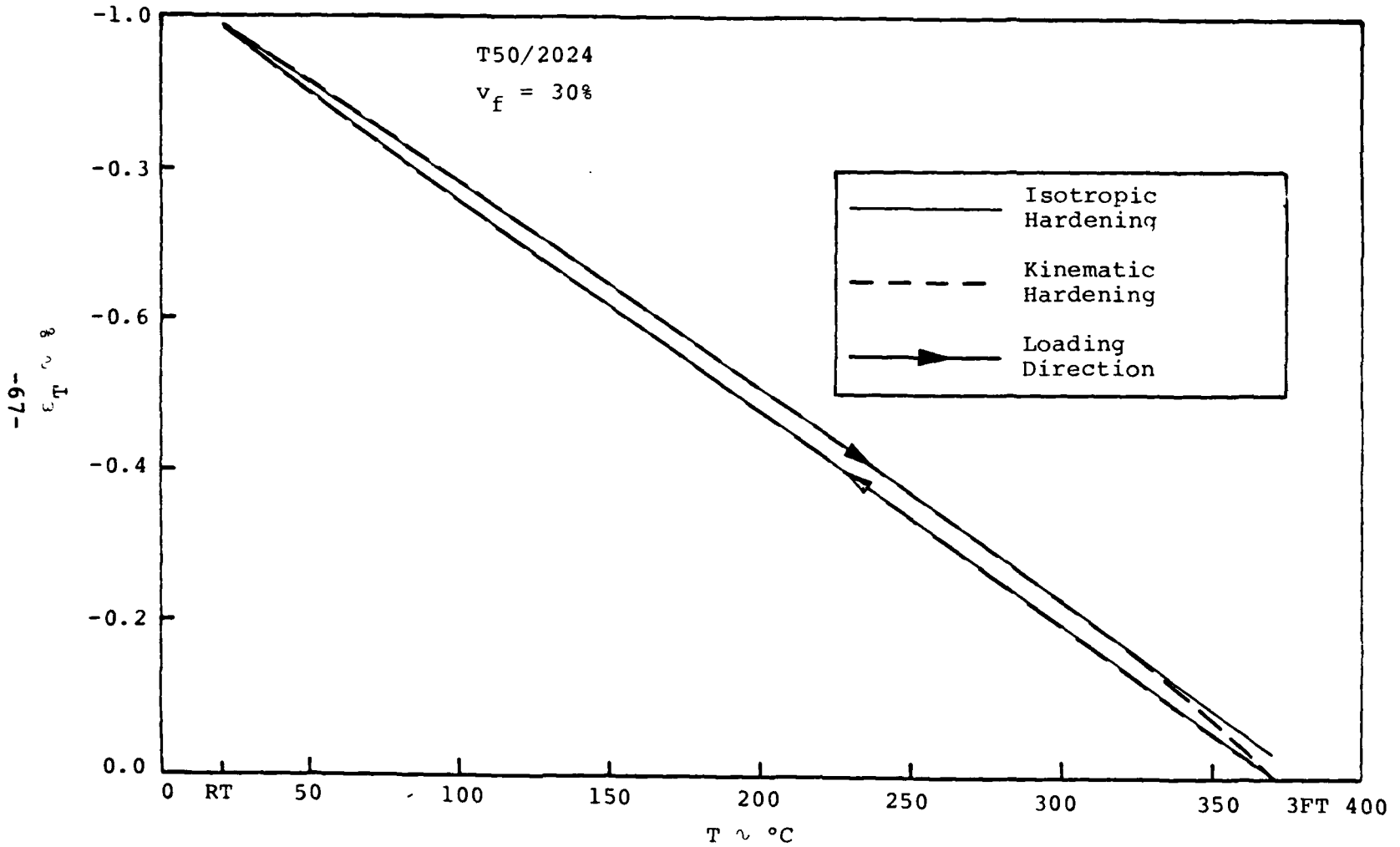

Figure 32. Transverse Thermal Expansion, Isotropic vs. Kinematic Hardening

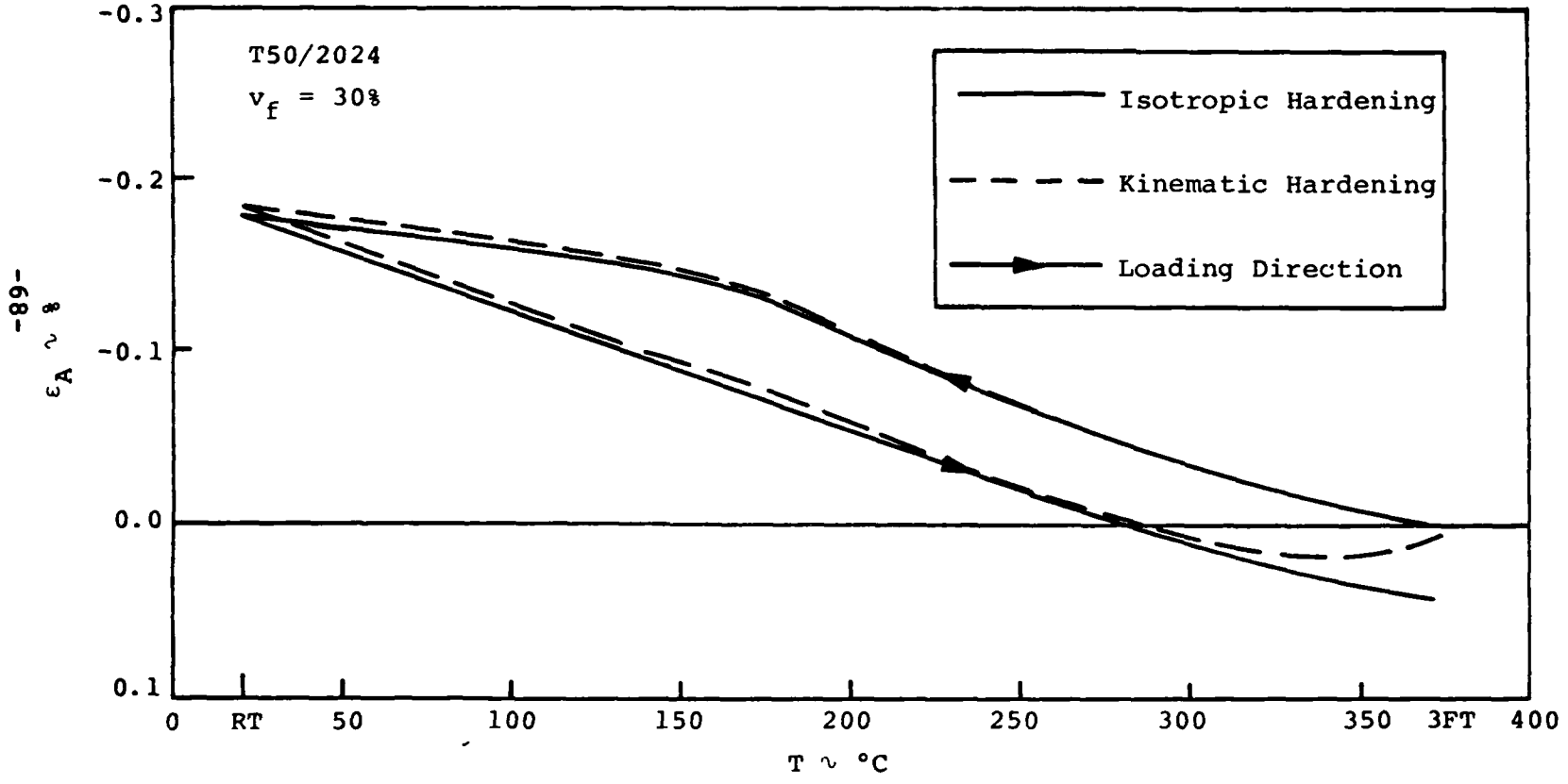

Figure 33. Axial Thermal Expansion, Isotropic vs. Kinematic Hardening

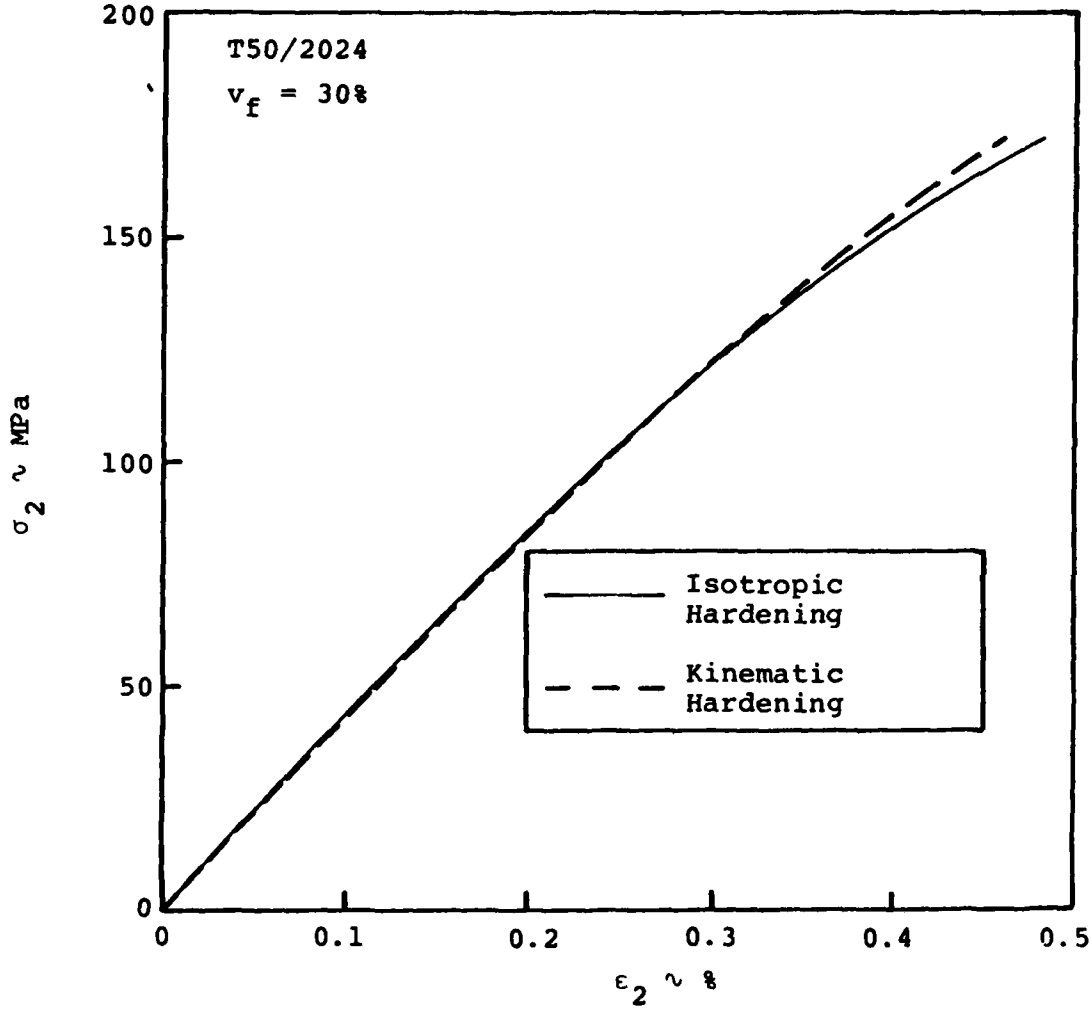

Figure 34. Transverse Stress-Strain Response at R.T., Isotropic vs. Kinematic Hardening

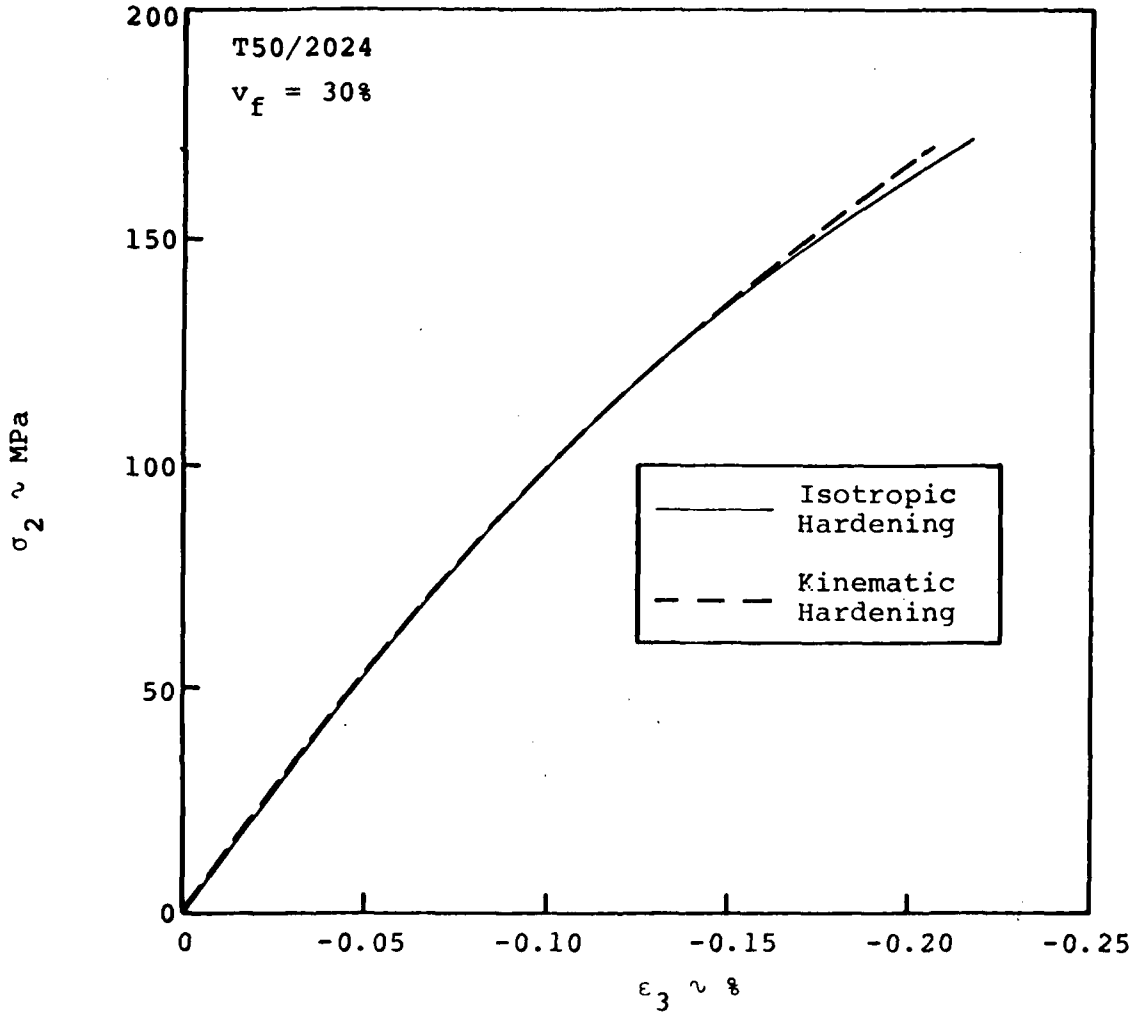

Figure 35. Transverse Normal Strain vs. Transverse Stress at R.T., Isotropic vs. Kinematic Hardening

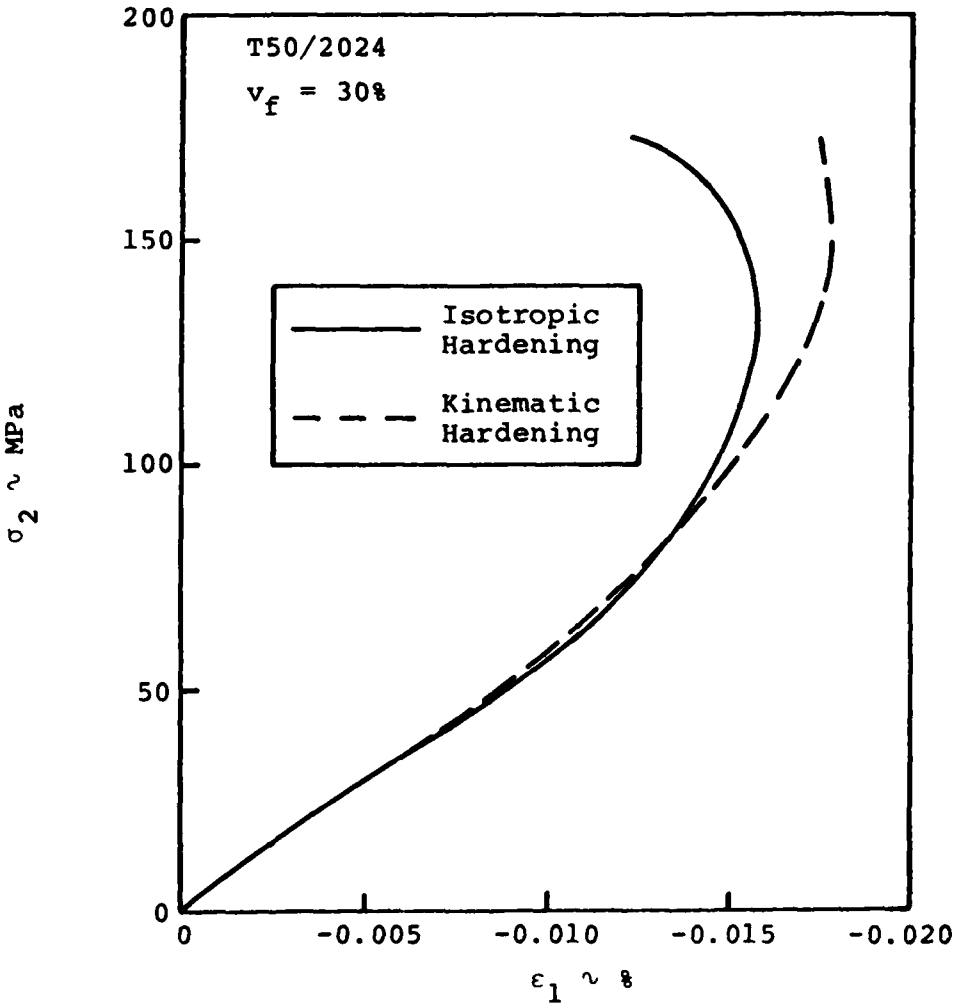

Figure 36. Axial Strain vs. Transverse Stress at R.T., Isotropic vs. Kinematic Hardening

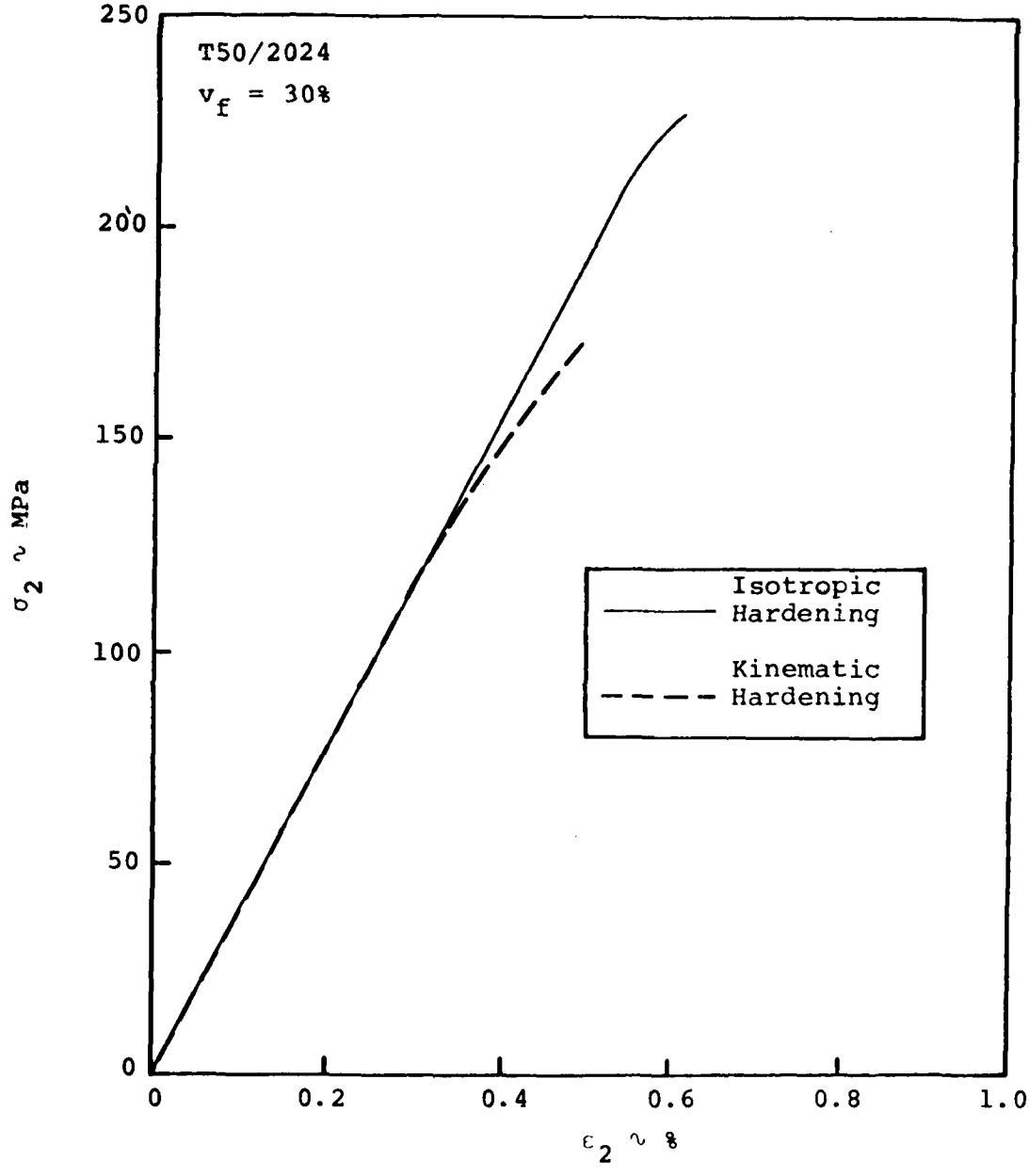

Figure 37. Transverse Stress-Strain Response at 204°C, Isotropic vs. Kinematic Hardening

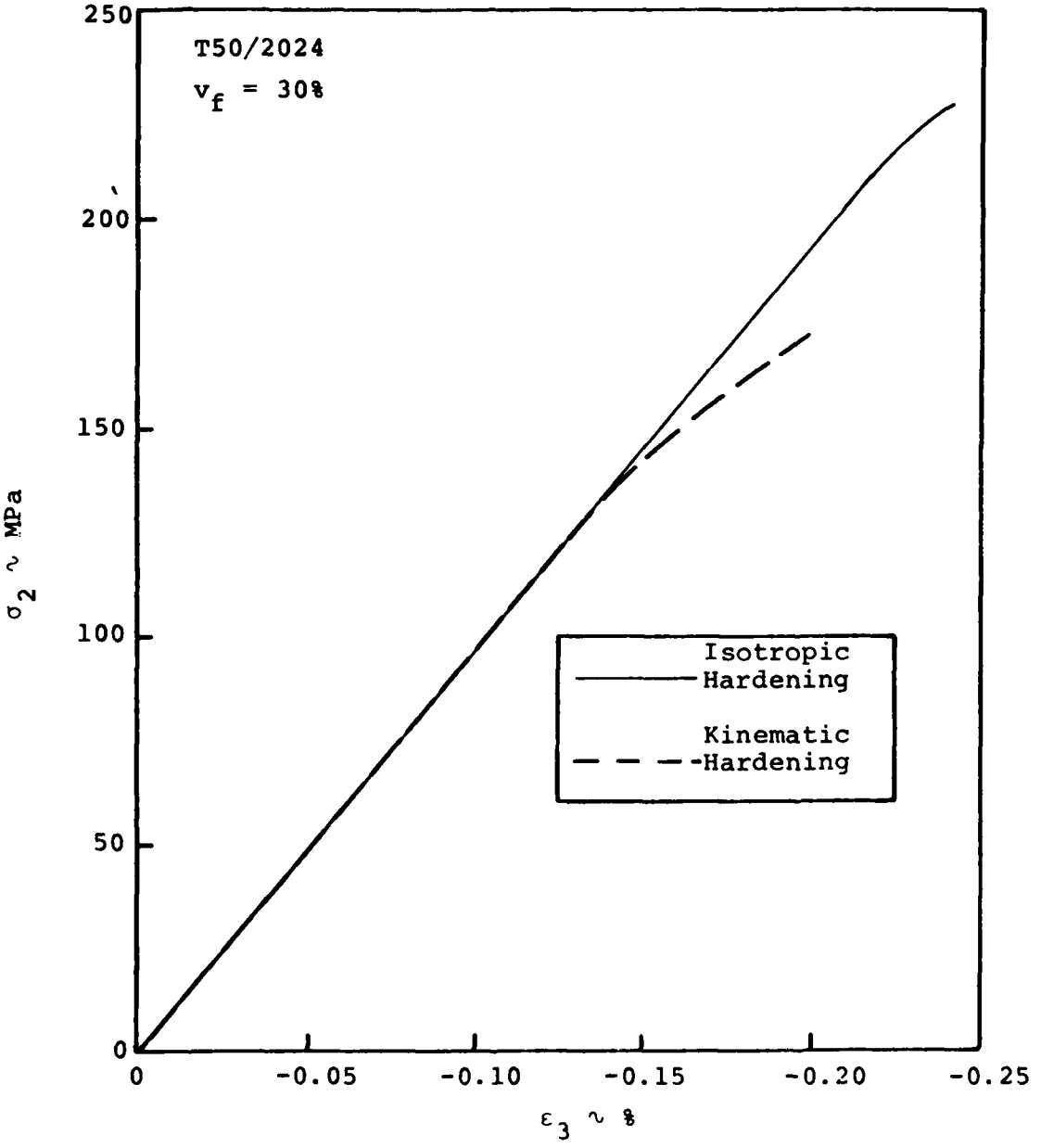

Figure 38. Transverse Normal Strain vs. Transverse Stress at 204°C, Isotropic vs. Kinematic Hardening

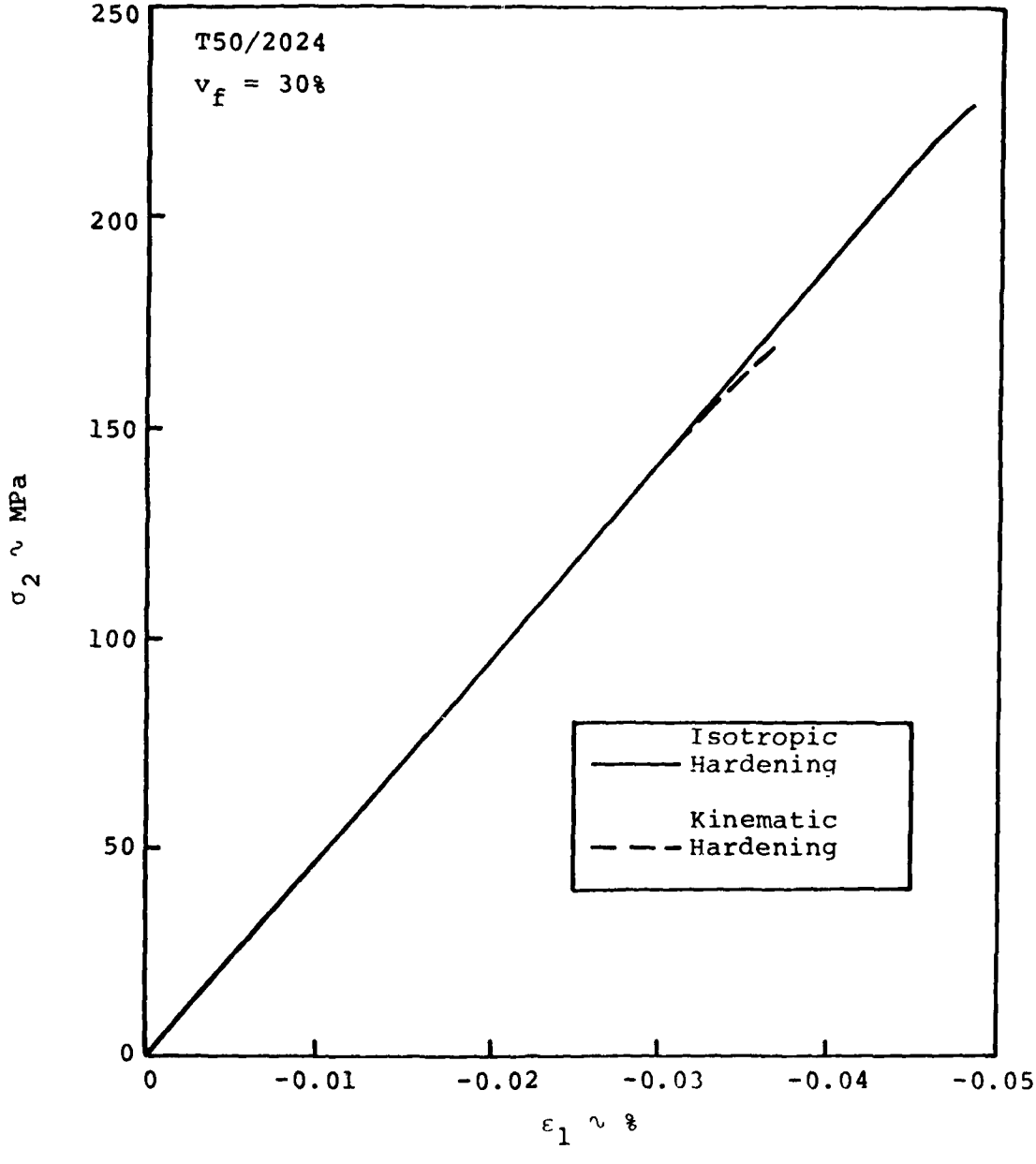

Figure 39. Axial Strain vs. Transverse Stress at 204°C, Isotropic vs. Kinematic Hardening

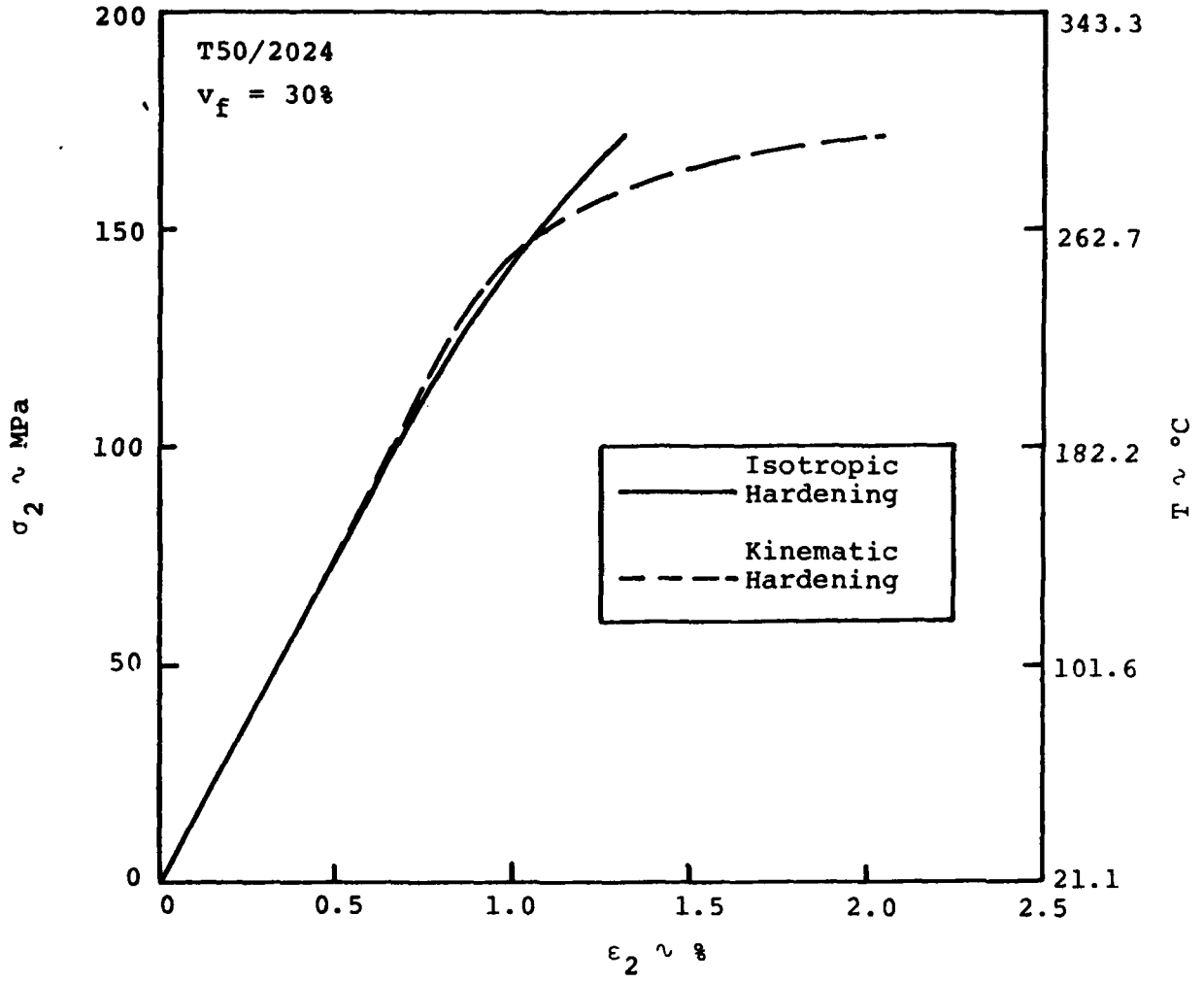

Figure 40. Proportional Simultaneous Variations of Transverse Tension and Temperature, Isotropic vs. Kinematic Hardening

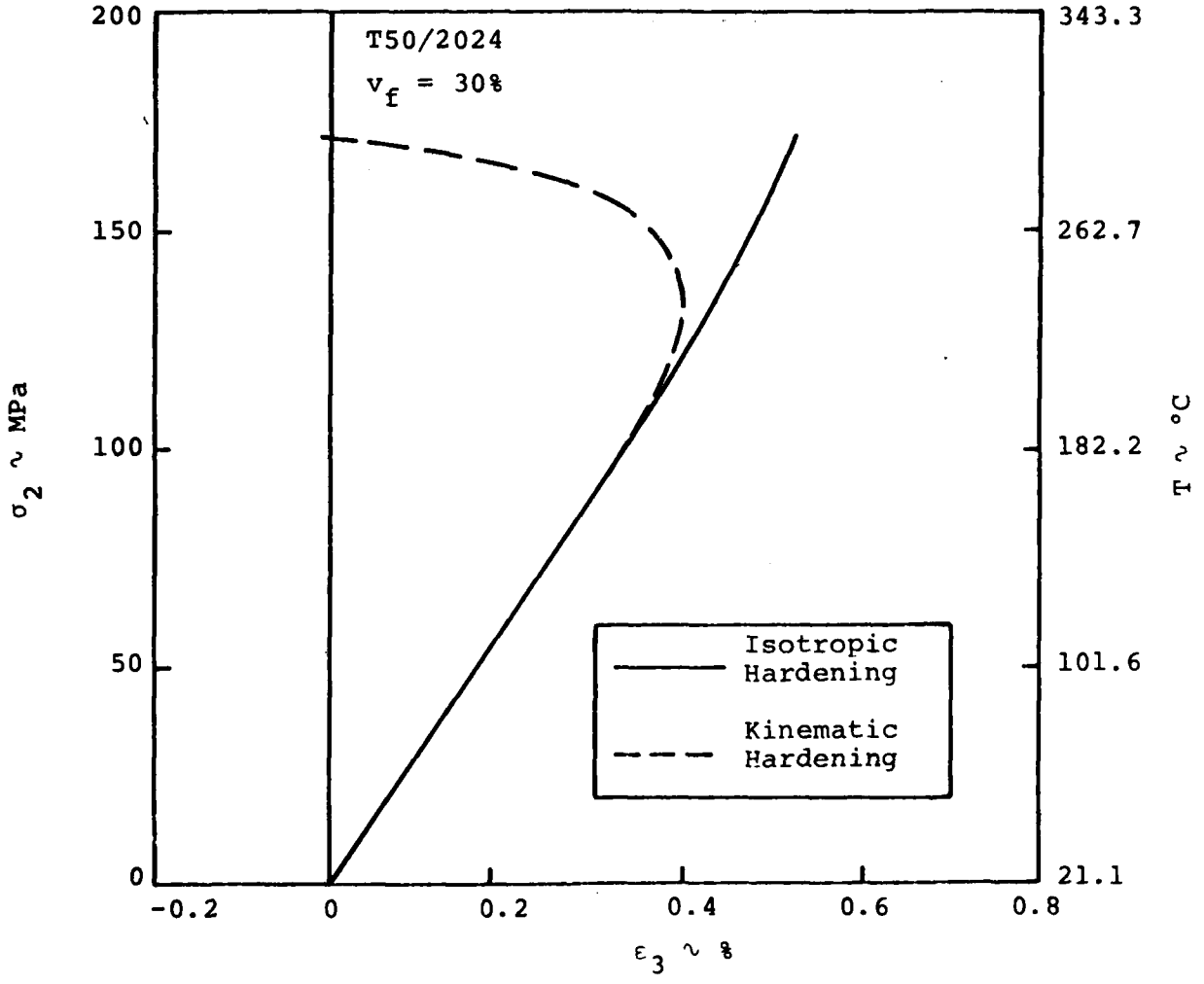

Figure 41. Proportional Simultaneous Variation of Transverse Tension and Temperature, Poisson Induced Transverse Strains, Isotropic vs. Kinematic Hardening

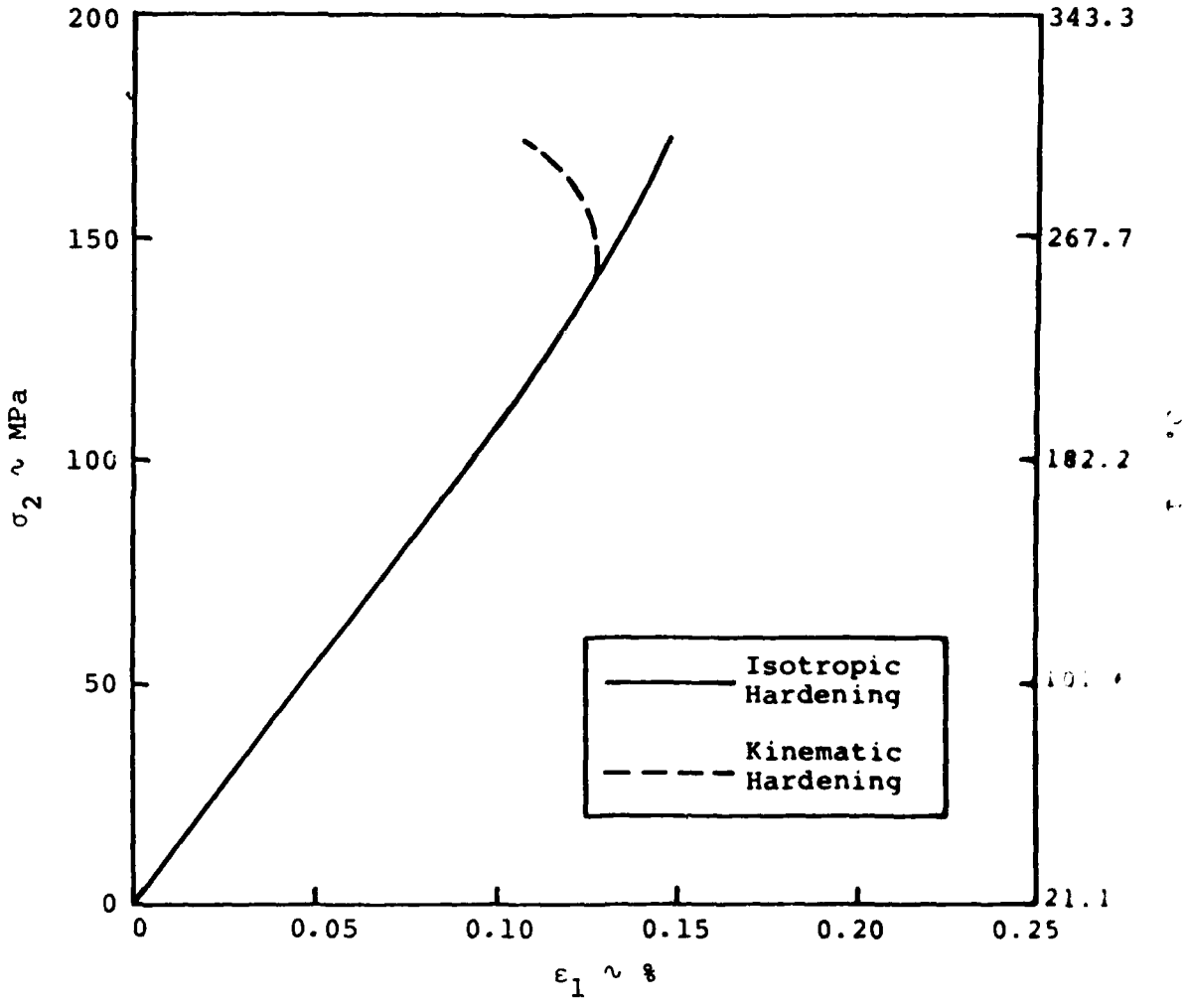

Figure 42. Proportional Simultaneous Variations of Transverse Tension and Temperature, Poisson Induced Axial Strains, Isotropic vs. Kinematic Hardening


DATE
FILMED
0-8